



University of
**Southern
Queensland**

**THE DETECTION AND ANALYSIS OF
IRRIGATION CHANNEL LEAKAGE
USING IMAGING FROM
AN UNMANNED AERIAL VEHICLE.**

A Thesis submitted by

Neville Madden, B Soc Sci, B Sci, Dip IT

For the award of

Master of Science

2022

ABSTRACT

In most major irrigation systems throughout the world the transport of water is via open irrigation channels and due to cost factors of enclosing or piping these open channels, this system will remain as the accepted method into the future. Water is one of the most vital commodities around the world but considerable quantities are lost daily through leaking, evaporation or broken channels. Leakage sites, called hot spots, along irrigation channels are usually wetter and contain lush vegetation than surrounding areas. Until recently the potential to use Unmanned Aerial Vehicles (UAV) was not a major component of resource management; however, this is rapidly changing due to better acceptance of the quality of information that can be collected by a UAV, the speed that which this information can be acquired and the cost savings that are immediately evident. This project has shown that leak detection using UAV fitted with a multi-spectral camera and using currently available software can be quickly and cheaply performed. This will help save considerable volumes of precious water lost to leakage. The saving of time and money by using UAV compared with routine inspections by paid labour will be considerable. Early leak detection will also allow for early repair of leaking irrigation channels and avoid catastrophic collapse of irrigation channel walls with the consequent flooding problems and loss of large amounts of scarce water. This study discusses the advantages and limitations of UAVs to detect irrigation channel leaks together with the results obtained and the benefits or problems experienced in processing the data obtained from the UAV flights.

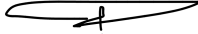
CERTIFICATION OF THESIS

I, Neville Richard MADDEN declare that the MSc Thesis entitled The Detection and Analysis of Irrigation Channel Leakage Using Imaging from an Unmanned Aerial Vehicle is not more than 100,000 words in length including quotes and exclusive of tables, figures, appendices, bibliography, references, and footnotes. The thesis contains no material that has been submitted previously, in whole or in part, for the award of any other academic degree or diploma. Except where otherwise indicated, this thesis is my own work.

Date: 17 Aug 2022

Endorsed by:

Dr Zahra Gharineiat, Associate Professor (Surveying and Positioning)

Principal Supervisor 

Dr Glenn Campbell, Associate Professor (Surveying)

Associate Supervisor

ACKNOWLEDGEMENTS

I would like to show my appreciation to the University of Southern Queensland who supported me financially for this project and provided me with the equipment to help understand the problems of UAV flying.

Next, I would like to thank my Principal Supervisor, A/Prof. Zahra Gharineiat. She has done more than just be my supervisor but has been a wealth of knowledge and has helped me learn the complexities of this project. For this I am grateful.

Thanks must go to Rohan Thorogood, the General Manager of Mallowa Irrigation Limited at St George and to Amanda Hicks, his capable assistant. They both have been extremely supportive and interested in this project. Without their help this project would have never started.

Last thanks must go to my wife, Rosemarie who not only proof read all my written submissions but supported me fully in this project.

Table of Contents

1. CHAPTER 1: INTRODUCTION.....	1
1.1 Aims and Objectives of this Project.	1
1.2 Scope of the Research.....	2
1.3 Background.....	2
1.3.1 How Can Early Detection of Irrigation Channel Leaks Save Money?	2
1.4 Elements of the Problem of Irrigation Channel Leakage	2
1.4.1 Problem Components.....	2
1.4.2 Identifying the Problem.	3
1.5 Loss of Water in Irrigation Channels.....	4
1.6 Study Area	5
1.7 Climate and Demographics of St George Region.....	6
1.7.1 Climate of the St George Region.....	6
1.7.2 Demographics, Land Use and Soil Types of the St George Region. 6	
1.7.3 What Happens If There is No Irrigation Water Allocated to Farmers?	8
1.7.4 Beardmore Dam Water Levels	10
1.8 Time Constraints to UAV flights.....	12
1.8.1 Factors For Supporting the Choice of Channel B2 for the UAV Flight	16
1.9 Satellite Images.....	17
1.9.1 Satellite Images Used.....	17
2 CHAPTER 2: LITERATURE REVIEW.....	18
2.1 Use of Unmanned Aerial Vehicles for Leak Detection.	18
2.1.1 Literature Related to Detection of Irrigation Channel Leakage by UAV.....	18
2.1.2 Other Projects Related to Irrigation Channel Leak Detection	22
2.1.3 Estimation of Irrigation Channel Losses Due to Seepage	26
2.1.4 Benefits of the Use of UAV in Agriculture	27
2.1.5 Other Uses for UAV	27
2.1.6 Use of Green Normalized Difference Vegetation Index Compared with Other Radiometric Vegetation Indices	28
2.1.7 Comparison of Vegetation Indices.	29

2.1.8	Relationship Between GNDVI Values and Chl-a Values	32
2.2	Current Methods of Leak Detection	32
2.2.1	UAV can Produce Better Results than Images from a Satellite	33
2.2.2	Use of Infra-red Imaging	35
3	CHAPTER 3: DATA and METHODOLOGY	38
3.1	Introduction.....	38
3.2	Pre-flight Preparation.....	38
3.2.1	Software Identification and Installation.....	38
3.2.2	UAV DETAILS.	38
3.2.3	Radio-metric Calibration of DJI P4 4 UAV.	40
3.2.4	Flow Chart for the Process of Irrigation Channel Leak Detection .	41
3.2.5	Pre-flight Planning	41
3.2.6	Satellites required by the UAV	43
3.2.7	Global Navigation Systems Used to Control the UAV	44
3.2.8	Proposed UAV Flight Parameters.....	44
3.2.9	Field Checking of Downloaded Data from UAV.	45
3.2.10	Production of the Ortho-Photo-Mosaic.....	45
3.2.11	Components of the Ortho-Photo-Mosaic Image.....	47
3.2.12	Processing the Ortho-Photo-Mosaic Using the European Space Agency's SNAP Toolkit	48
3.3	Mask overlays	49
3.3.1	Use of High Chlorophyll-a mask	49
3.4	Creating the GNDVI Hotspot Maps and Confirmation of Hotspots	54
3.4.1	Preparation of Hotspot Location Map.	54
3.4.2	Confirmation of Leakage Hotspots.....	54
3.4.3	Ground Truthing Control Holes.....	55
3.4.4	Ground-truthing Procedure.	55
3.4.5	Unified Soil Classification System.....	56
3.5	Other Considerations	58
3.5.1	Risk Assessment	58
3.5.2	Insurance and WH&S Equipment Provisions.....	58
3.5.3	Notification to Landowners of Proposed Flights.....	58
3.5.4	Aerial Crop Sprayers and Civilian Aircraft	59
4	CHAPTER 4: RESULTS and DISCUSSION	60

4.1	Introduction.....	60
4.2	ST GEORGE – PHASE 1 – 9 APRIL 2021.	60
4.2.1	Factors Affecting the Possible Outcomes	60
4.3	The UAV Flights	64
4.3.1	UAV Flight Procedure	64
4.4	Suitability of the DJI P4 UAV for This Project and Flight Times	66
4.4.1	Suitability.....	66
4.4.2	Flight Time	66
4.5	Processing of UAV Images.....	67
4.5.1	Production of Ortho-Photo-Mosaic Images	67
4.6	Production of the GNDVI Overlay and Masks.....	68
4.7	Plotting the Hotspots on a Map	71
4.8	SMC from Ground-truthing, USC Classes and Munsell Colours.....	74
4.9	Soil Classification Results.	76
4.10	Control Points	76
4.11	Results St George – Phase 2 – April 2022.....	76
4.11.1	Factors Affecting Possible Outcome	76
4.12	Risk Assessment for Phase 2 Flights and WH&S Induction	79
4.13	The UAV Flights	79
4.13.1	UAV Flight Procedure	79
4.14	Suitability of the University’s NEW DJI P4 UAV	80
4.15	Flight Times, the Use of Real Time Kinetics System and Flight Patterns .	81
4.16	Processing of UAV Images.....	81
4.16.1	Production of the Ortho-Photo-Mosaic Images	81
4.16.2	Production of GNDVI Overlay.....	83
4.16.3	Calculating GNDVI Values Using the Mask System in the European Space Agency’s SNAP Toolbox.....	84
4.16.4	Plotting the Results on a Map.....	85
4.16.5	Potential Leak Site Identifications	90
4.16.6	Variation in Munsell Colours from Phase 1	92
4.16.7	Interpretation of Data from Table 8.....	93
4.16.8	Influence of Recent Heavy Rainfall.....	93
4.16.9	Soil Classification Results	94
4.17	Use of alternate radiometric vegetation indices.....	94

4.17.1	Selection of Appropriate Radiometric Vegetation Indices	94
4.18	Other Software Applications that Produce Vegetation Indices	100
4.18.1	Other Applications	100
4.18.2	Summary of Other Applications to Produce Vegetation Indices..	102
4.19	Discussion	102
4.19.1	Variation in Hotspot Count Between Phase 1 and Phase 2	102
4.19.2	Discussion About this project	102
4.19.3	Satellite Imagery Comparisons	104
5	CHAPTER 5: CONCLUSION	105
5.1	Functionality of the System.	105
5.1.1	Did the System Work?	105
5.1.2	Confirmation of the UAV's Effectiveness.....	105
5.1.3	Effects of Soil Type on Potential Irrigation Channel Leaks	106
5.1.4	Future Work.....	106
6	REFERENCES	108

1. CHAPTER 1: INTRODUCTION

1.1 Aims and Objectives of this Project.

The aim of this project is to develop a functioning system for the fast, accurate and cost efficient detection of potential irrigation channel leakage. To achieve this aim, the system with the highest potential to reach these parameters will be one that can use Unmanned Aerial Vehicles (UAV) fitted with a multispectral camera. The images resulting from the UAV flight should be easily and rapidly processed using software applications to define any potential leakage site in an irrigation channel. The system that this project proposes has the potential to detect potential leakage sites in an irrigation channel, quickly, cheaply, effectively, with the use of a minimal number of personnel there-by making it a cost-effective system.

The objective s of this program are:

1. Plan and fly a series of UAV flights to collect images of irrigation channels,
2. Process those images into a format that commercial software can evaluate and provide usable information on potential irrigation channel leakage sites,
3. Utilize the processed data to produce usable maps with the location of all potential leakage sites and,
4. Maintain the highest standards of accuracy that the available software and equipment can provide.

1.2 Scope of the Research

This research is intended to produce a viable, economical and timely solution for the world-wide detection of potential irrigation channel leakage sites. This proposed system can be used on all types of irrigation channels and drains in any complex.

1.3 Background

1.3.1 How Can Early Detection of Irrigation Channel Leaks Save Money?

Australia is an extremely dry continent with most rainfall occurring on the coastal fringes. Away from the coast any water that is available for irrigation is a precious commodity and needs to be conserved so that the maximum benefit of irrigation water can be shared by all irrigators. Water costs money and any loss of irrigation water means a financial loss to the irrigation system management, together with increased costs to the irrigator to compensate for these losses. The Mallowa irrigation system at St George, Queensland's 2023 pricing for water is \$35.45 per ML (Mallowa Irrigation Ltd., 2022).

1.4 Elements of the Problem of Irrigation Channel Leakage

1.4.1 Problem Components

It is necessary to look at three components of the problem where irrigation water losses are occurring.

They are:

1. identifying the problem,
2. producing a possible solution and,

3. evaluating the effectiveness of the solution (Mohommadi et al., 2019)

1.4.2 Identifying the Problem.

At present, identifying the problem of irrigation channel leakage can be as simple as locating a visible leak and the associated presence of lush, green vegetation during a physical inspection. Another method is that an irrigator reports to the irrigation management that the crops at a particular location are being water-logged due to an irrigation channel leak. A more complex system but one which may be more accurate is to use photographic images supported by a system of interpretation to identify potential leaks in irrigation channels. These images can either come from high resolution satellite photos or an UAV or commonly known as a drone.

1.4.2.1 Producing a Possible Solution.

Over-flying the irrigation channel with an UAV fitted with the appropriate cameras and collecting photographic images for later manipulation may provide a fast, efficient and cost-effective solution to the problem.

1.4.2.2 Evaluating the Effectiveness of the Solution.

The effectiveness of the proposed solution can be measured by the ability of the adopted system to detect and identify the sites of existing or potential irrigation channel leakage.

1.4.2.3 Identifying Problems in Any Possible Solutions.

The problems associated with the possible solution are:

1. regular visual inspections are time consuming and this equals increased costs to the irrigation management,
2. high resolution satellite imagery, with Ground Spatial Distances (GSD) less than 1 m, is expensive. It may have cloud cover and may take weeks before a clear image is available and,
3. UAV mapping has high spatial resolution but may lack a required temporal resolution. In other words, it may not available at the required time or needs to be scheduled to be performed on a frequent basis.

1.5 Loss of Water in Irrigation Channels

All unlined channels lose water through seepage. In the Murray-Goulburn Irrigation system in Northern Victoria, for every one kilometer of three meter wide channels this leakage loss equates to 4.5Ml loss per km per km/day, or 16.5 Gl/day for the 4166 km of irrigation channels in the hottest periods of the year, (P. King, personal communication, 12 May 2021). With water costing \$21 a Ml this is a massive loss of \$16,500 just through seepage each day. It is estimated that evaporation losses are up to four times the normal seepage losses (Goulburn-Murray Water, 2012).

With such high potential losses and water being such a scarce commodity in Australia early detection and remediation of any potential irrigation channel leakage is essential. This project intends to introduce a new, cheaper and accurate system of leak detection in irrigation channels.

1.6 Study Area

It was decided to undertake two research projects in St George; one year apart. This would have the same location parameter but possibly with different vegetation variables due to high rainfall between November 2021 and April 2022 (Australian Bureau of Meteorology, 2020a).

Figure 1

Location of St George Queensland.



Note: Source – (Department of Natural Resources, Mines and Energy, 2017; Geoscience Australia, 2019).

1.7 Climate and Demographics of St George Region

1.7.1 Climate of the St George Region

In the St George region evaporation during the summer months is high. The Koppen-Geiger classification (Chen, 2023) for the region under study is BSh (Hot, semi-arid Steppe Climate) with summer temperatures reaching 47.2⁰ C at St George, Queensland on 3 January, 2014 (Elders Limited, 2022). The quantity of water losses through seepage or evaporation were not available from Mallowa Irrigation Ltd.

Data from the Australian Bureau of Meteorology for St George Airport from 1997 to early May 2021 show the annual mean rainfall is only 459 mm. Most of this rain falls during summer and early autumn (Australian Bureau of Meteorology, 2020a). Often this rainfall phenomenon is caused by the effects of the Indian Ocean Dipole (IOD). During this event, a large mass of warmer water moves backwards and forwards across the Indian Ocean; similar to the El Nino Southern Oscillation (ENSO) on the nation's east coast. When the IOD is in a negative mode a large body of warm water lies close to the West Australian coast. With this warm water comes increased evaporation, stronger westerly winds and increased cloud cover over inland Australia with the potential for rain to fall across inland Queensland (Australian Bureau of Meteorology, 2020b).

1.7.2 Demographics, Land Use and Soil Types of the St George Region

The 2016 Census showed the population of St George and surrounding districts to be 3048 (Australian Bureau of Statistics, 2016). This area's agriculture is predominantly cotton growing on black basalt soil, using irrigation water. Outside of the irrigated

cotton growing area the main pastoral usage is for beef cattle. The Queensland Government’s Soil Association Map shows that the majority of the irrigation channel system are within the zone of “Deep grey or grey brown calcareous heavy clay” (Queensland Irrigation and Water Supply Commission, 2014). However, this area, as the result of irrigation water being available, is now used predominantly for cotton growing when full water allocations are available. An image of irrigation channel B2 (Bundoran Road) is shown as Figure 2, while a row of harvested cotton bales is shown as figure 3.

Figure 2

Bundoran Road Channel (Channel B2)



Note: Irrigation channel at register point, Dethridge Wheel for water delivery measurements at left and cotton ready for harvest at right. Own photo 13 Apr 2022.

Figure 3

Harvested cotton



Note: Own photo 12 April 2022.

1.7.3 What Happens If There is No Irrigation Water Allocated to Farmers?

When water is unavailable for irrigation due to low water level in Beardmore Dam the cotton growers that rely on this water often plant Mung Beans or Chick peas in lighter soils on their properties (Butterworth, 2016). Beardmore Dam is shown at Figure 4, where the dam is at 60% capacity and the Thuraggi Channel outlet is shown in Figure 5. In February and March 2021 Beardmore Dam overflowed following high rainfall level in the catchment of the Condamine River; near Warwick Queensland (Sunwater, Queensland, 2021). The Condamine River meanders through the Darling Downs and

joins the Balonne River near Surat on the western Darling Downs. Beardmore Dam is located on the Balonne River, 14km north of the town of St George.

Figure 4

Beardmore Dam at 60% capacity



Note: Own photo April 2021.

Originally the irrigation water was drawn from Jack Taylor Weir, built across the Balonne River, near the centre of St George, in 1953. This weir was built primarily for town water and is still in use for that purpose today. Water is also fed into the irrigation channel systems from this location. This is one of the two locations where water enters the system. As the need for more water for irrigation increased the Queensland Government decided to build Beardmore Dam in 1972. Water from this dam enters the Thuraggi Channel and flows into the eastern side of the irrigation channel system at

Buckinbah Weir. Thuraggi Channel and main channels are shown below as Figure 5. All of the channels are open earth construction, without any lining and are fully gravity operated. The majority of the irrigation channels have been constructed above ground level. There are manually operated flow control systems to meet irrigator's crop demands (SunWater, 2021).

Figure 5

Thuraggi Channel at 100% capacity.



Note: Source – Bing Maps and SAS.Planet (SAS.Planet Development Team (2022 and (Blue Marble Geographics, 2021).

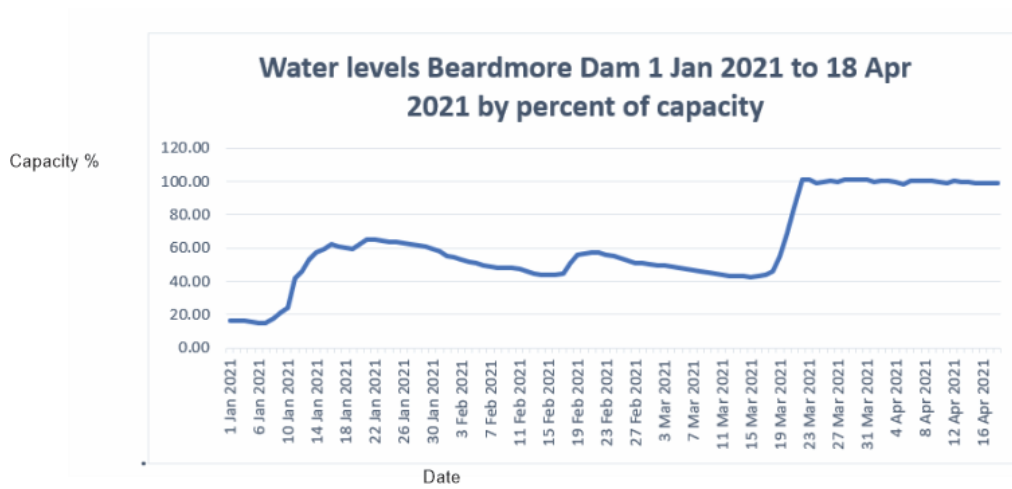
1.7.4 Beardmore Dam Water Levels

The irrigation system relies on high dam water levels. Beardmore Dam water levels are shown in Figure 6, for 2021 and Figure 7 for 2022. Beardmore Dam overflowed on 22 Mar 2021 as the result of high-water levels in the Condamine River. This dam maintained full water levels up until 17 Apr 2021 when the dam levels fell steadily due to distribution of water into the irrigation channel system (Sunwater Queensland, 2021). The high water levels in Beardmore Dam will guarantee that all the irrigation

channels in the system will be filled to maximum capacity, providing an alternate storage location for the surplus water. This will aid the detection of potential leak sites along the irrigation channels.

Figure 6

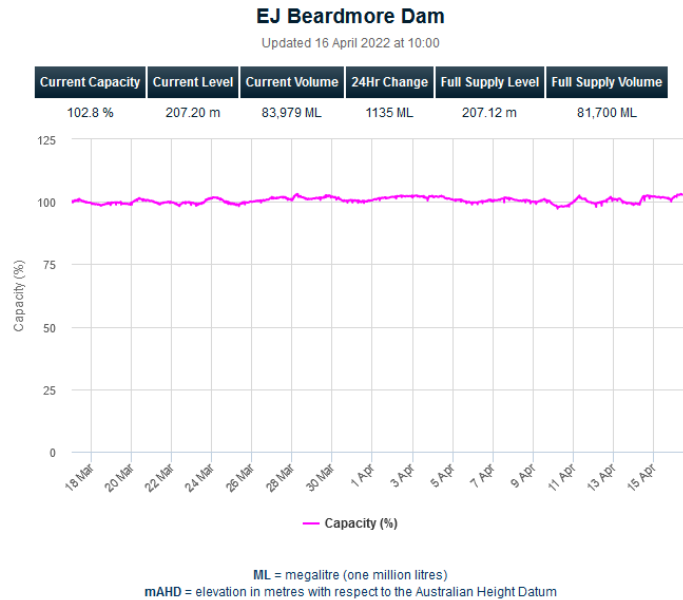
Water levels - Beardmore Dam, 2021



Note: Source: From SunWater Water Supply Schemes (Sunwater, Queensland, 2021).

Figure 7

Water levels - Beardmore Dam, 2022



Note: From SunWater Water Supply Schemes (Sunwater, Queensland, 2022).

Management of this irrigation channel system passed on 1 July 2018 from SunWater Queensland, a quasi-Government entity, to Mallowa Irrigation Limited, an irrigator owned co-operative organisation that manages 112 km of irrigation channels, with 50 irrigators who irrigate ten thousand hectares of cotton (Mallowa Irrigation Limited, 2018).

1.8 Time Constraints to UAV flights

The licenced CASA contractor that donated his services in April 2021 could only allocate one day of UAV flying to this project. In April 2022 a CASA licenced flight operator from a commercial company was contracted by the School of Survey, University of Southern Queensland, Springfield Campus. In the first instance, during

2021, flights were restricted to what could be performed on one day. In April 2022 two days were allocated to the project and although all work was completed on day one, the photography for Flight Path Five and Six had to be re-done due to tree shadows covering the flight path. Consequently, this project has only been able to conduct UAV flight operations over the Bundoran Road channel (B2). This is shown on Figure 8 below, highlighted in yellow.

The flight path used in April 2021 is shown in Figure 8. All of Bundoran Road channel (Channel B2) was flown. In April 2022 the flights were flown over sections BDA Flt Paths 1,4,5,6,7and 8 as shown in Figure 9. BDA Flt Paths 2 and 3 were eliminated following a visual safety inspection that included, trees, power-lines and residences prior to commencement of flights. The areas eliminated had been recently mown and Mallawa Irrigation Ltd., management reported that no leaks were identified during this mowing process.

Figure 8

Irrigation channel flights April 2021



Note: Base map Bing and (SAS Planet Development Team, 2021) and (Blue Marble Geographics, 2020).

Figure 9

Flight paths flown in April 2022



Legend

Flight Paths	
BDA Flt Path 1	BDA Flt Path 5
BDA Flt Path 2	BDA Flt Path 6
BDA Flt Path 3	BDA Flt Path 7
BDA Flt Path 4	BDA Flt Path 8

Note: Source- BING Satellite Map via SAS.Planet, 2022

Note: Base map Bing and (SAS Planet Development Team, 2021) and (Blue Marble Geographics, 2020).

1.8.1 Factors For Supporting the Choice of Channel B2 for the UAV Flight

Financial and time constraints for this project meant that these irrigation channels were chosen by Mallowa Irrigation Limited who advised that this irrigation channel, B2, had the greatest potential for leakage. Vehicle access along the total length of this channel is good and visible high green grass and weeds are visible on the satellite images shown in Figure 10 below.

Figure 10

Beginning of Channel B2, with high grass.



Note: Source BING satellite image via SAS software (SAS.Planet Development Team, 2021).

1.9 Satellite Images

1.9.1 Satellite Images Used

The satellite images in Figures 8, 9 and 10 are from the European Space Agency's Sentinel 2a and 2b satellites. These two satellites are components of the Copernicus satellite system. The Copernicus satellite system comprises seven Sentinel satellites (European Space Agency, 2022). For this project the images have been downloaded from the Sentinel 2b satellite using SAS.Planet software (SAS Planet Development Team, 2021). The Sentinel 2a and 2b satellite system is designed for land and sea observations. The polar orbit height is 740km and its strip-map swath is 290km wide. In the sample downloaded in Figure 10 each pixel is 9.96m wide. This is sufficient to identify green grass patches on the satellite images from the European Space Agency (European Space Agency (1), 2021 and SAS.Planet Development Team, 2021).

In the Copernicus series of satellites, the Sentinel 2a and 2b satellites are polar orbiting satellites and travel the same orbit path but 12 hours apart. Both satellites use multi-spectral sensors to image both the landforms and the ocean. They provide reliable, timely, frequent, radar imaging of both the land and all of the oceans. Some other satellites switch off when they pass over the ocean to save energy. When operated together these two satellites have a re-visit time of five days, with imagery downlink available within two days after each satellite pass.

2 CHAPTER 2: LITERATURE REVIEW

2.1 Use of Unmanned Aerial Vehicles for Leak Detection.

2.1.1 *Literature Related to Detection of Irrigation Channel Leakage by UAV*

An extensive search of published literature revealed a small quantity of papers that were specifically related to the use of UAVs for irrigation channel leak detection. The interpretation of this lack of published material suggests that the use of UAVs in this role was not world-wide. However, a large amount of information is available on the use of UAVs in agriculture and that some of this information is relevant to this project. After discussion on the specific use of UAVs for irrigation channel leak detection reference will be made to those related uses of UAVs in agriculture that may be relevant to this project.

The first journal article that specifically uses UAV to detect irrigation channel leakage is a study conducted in Sulawesi, Indonesia where a fixed single wing UAV was used to produce images for leak detection of the irrigation area under study (Ibrahim, J.T et al., 2017). This was done to identify leaking irrigation channels and assist with rice crop management. The flight was conducted at 140m above ground level with good side and forward overlap of the photographic images.

The flight operation produced normal red-green-blue images which were used for crop management while the Near Infra-Red (NIR), green and blue band images produced data for irrigation channel leakage determination. All images were used to create an ortho-photo-mosaic image of the flight paths.

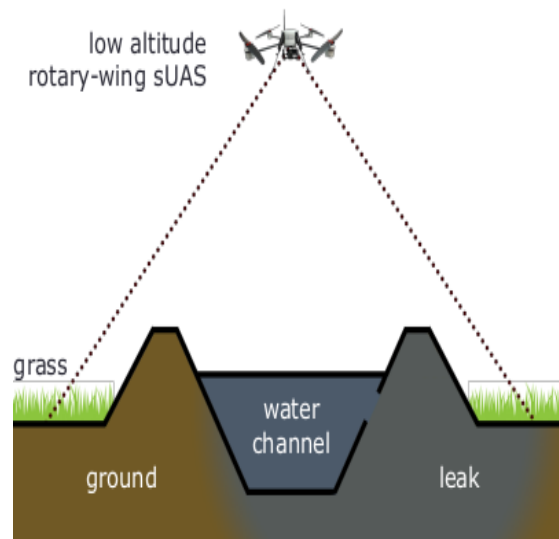
No count of the potential leakage spots was given but the authors felt that the system had a high potential to discover irrigation channel leaks (Ibrahim, J.T et al., 2017).

The second method was used by Texas A & M University (Dufek et al., 2017) along the Colorado River in Texas, USA. In 2017, Texas A & M University conducted trials using a multi-propellor Small UAV for irrigation channel leak detection. This Unmanned Aerial Vehicle was fitted with a MicroSense Red Edge Multi-spectral camera, a FLIR Vue Pro Thermal Camera and a CMOS Camera with 728 x 488-pixel resolution for normal photography. Seven leaks were detected in the irrigation channels that come off the Colorado River in Garwood, TX.

Unfortunately, the trials are subject to ‘Patent Pending’ and no further information is available (Dufek et al., 2017). The paper concludes that this method was considered successful but a search of the US Patent Office for the terms “Irrigation channel leak detection” and “Irrigation canal leak detection” did not produce any positive results (US Government, 2021). The flight concept used by Texas A &M University is shown in Figure 11 below.

Figure 11.

Texas A & M University's UAV program.



Note: From Detection and Localization of Irrigation Canal Leaks Using Small Unmanned Aerial Systems (sUAS) at Low Altitudes by Dufek et al from Texas A & M University (Dufek et al., 2017).

In the paper “Survey of Irrigation area using Micro Unmanned Aerial Vehicle (microUAV) in Gumbasa irrigation area” the authors discuss comparisons between Red-Green-Blue method and Near Infra-Red-Green-Blue (NirGB) methods and conclude that the use of micro-UAV at the location in Sulawesi, Indonesia, is an efficient process to evaluate a crop’s condition in an irrigated system. They also identified that the Near Infra-red-Green-Blue system may also have potential uses to detect irrigation channel leakage (Ibrahim, J.T et al., 2017).

The paper “Leak Detection in Water Transmission Systems by Multispectral Remote Sensing with Airplane and UAV,” by (Chatelard et al., 2019) has some factors that are related to this project. Both vehicles were fitted with a multi-spectral camera, sensing

in the red, green, blue and near infra-red bands and ortho-photo-mosaic registration was done using Gefolki software (Plyer, 2016/2023). This software produces similar results to Agisoft Metashape ®software used in this project. Each pixel of the ortho-photo-mosaic had its Normalized Digital Vegetation Index (NDVI) plotted and recorded (Chatelard et al., 2019). Where high NDVI values were met field detection was conducted and leaks were discovered. This use of vegetation indices is similar to the ones used in this project.

The authors of the journal article titled “Airborne remote sensing for the detection of irrigation canal leakage” (Huang et al., 2010) discuss how they used a multi-spectral imager equipped with red, near infra-red and thermal sensors, mounted on a low flying aircraft in the Lower Rio Grande Valley of Texas, USA. The process flew over 24 irrigation channel segments and assessment of the data obtained indicated 140 sites were potential irrigation channel leakage sites. Field examination confirmed that 26 of the 28 high potential irrigation channel leakage sites were actually leaking. Image processing was done using ERDAS Imagine and Leica Geo-systems Geospatial Imaging. The stages involved were:

1. Convert image from RAW to .IMG format
2. Register images for co-ordinates,
3. Combine red, NIR and thermal images into one composite image,
4. Geo-reference images using identified ground control points,
5. Crop images to area-of interest and
6. Calculate NDVI and plot values.

Field reconnaissance was conducted after the production of a GIS map. The procedures used in this project are similar to the proposed project at St George but a lot of the work done in the stages listed above can be done much simply using Agisoft Metashape ® software and the open-source SNAP Toolkit from the European Space Agency (Agisoft LLC, 2022; European Space Agency, 2020)

2.1.2 Other Projects Related to Irrigation Channel Leak Detection

“Identifying Potential Leakage Zones in an Irrigation Supply Channel by Mapping Soil Properties Using Electromagnetic Induction, Inversion Modelling and a Support Vector Machine” is a journal article based on the detection of irrigation channel leaks in the Namoi Valley, NSW cotton growing area (Zare et al., 2020). In this project a DUALEM-421 sensor was used to measure electrical conductivity along a section of irrigation channel.

“A DUALEM sensor incorporates one-, two- or three-sets of the patented DUALEM dual-geometry array. Each dual-geometry array simultaneously measures both electrical conductivity and magnetic susceptibility to two distinct and defined depths” (DuaLEM Inc., 2022, para 1).

The sensor was mounted on wheels and towed along the irrigation channel bank. Where anomalies were recorded the location was geo- referenced using a GPS and a soil sample collected at 0.5m increments to a maximum depth of 6.0m. Using the EM4 soil inversion software (EMTOMO, 2023) the user was able to detect locations of low clay content. These locations suggest that irrigation channel leakage is occurring due to the dissolution of clay particles in the irrigation channel base and banks.

Huang et al (Huang et al., 2016) conducted an almost identical project but at Riverside County, Southern California in 2015 except that the data produced was used for irrigation management of a lucerne crop.

When using Satellite imagery to make an assessment of Aquatic Weeds, researchers from Deakin University in Victoria found that with satellite images they had to undertake co-registration of images, atmospheric correction, band statistic calculations and clustering together with supervised and unsupervised classification. They then used a UAV with a red-green-blue camera and achieved similar results but with a GSD of five cm/pixel, compared to the 30cm pixel resolution from pan-sharpened images from the World-View 3 satellite constellations. The UAV data required less processing, using a commercial image processing software application and this allowed the users to differentiate between the different aquatic weed types (Brinkhoff et al., 2018).

(Bian et al., 2019) wrote their paper “Simplified Evaluation of Cotton Water Stress Using High Resolution Unmanned Aerial Vehicle Thermal Imagery” on how they used thermal imagery collected by a UAV to calculate the Crop Water Stress Index (CWSI) of a cotton crop. Crop canopy temperatures were collected and used to calculate the CWSI and used as a parameter for accurate irrigation management. This procedure has the potential to be used as an alternate method of irrigation channel leak detection by evaluating CWSI values of grasses at potential irrigation channel leaks compared with surrounding vegetation (Bian et al., 2019).

“Mapping Very-High-Resolution Evapotranspiration from Unmanned Aerial Vehicle (UAV) Imagery” is a paper by (Park et al., 2021). It discusses the use of an UAV to map and collect imagery, both thermal and digital with a Ground Spatial Distance of

<8cm. This imagery was then processed using the high-resolution mapping of an evapo-transpiration model, developed by the University of Melbourne and a tree-by-tree evapotranspiration map was produced (Park et al., 2021). Although not directly related to this project the methods used have the potential to be used for further work on detection of irrigation channel leakage detection.

The journal article “Using multi-satellite microwave remote sensing observations for retrieval of daily surface soil moisture across China” (Zhang et al., 2019) provides interesting insights as to a method of detecting SMC but, without detailing the process, it was found that the results obtained covered too wide an area to be a viable source of accurate locations of potential leak sites in irrigation channels.

Agapiou et al write in their paper “Investigation of Ground Remote Sensing Techniques for Supporting an Early Warning Water-Leakage System” about the use of satellites, particularly Landsat 7 and SPOT-5 to provide data from remote airborne sensing, using vegetation indices that can be used to calculate soil moisture content (SMC) and vegetation biomass using thermal sensing. This data from thermal cameras gives indications that the subject area is water, very wet, wet or dry allowing a determination of the SMC and potential leak site. This process was used to detect leakage in underground pipes systems with 91% accuracy. Multiple vegetation indices were applied and the NDVI and its derivatives such as the Green Normalized Vegetation Index (GNDVI) were seen to produce the best results (Agapiou et al., 2014). This project will confirm that the GNDVI is the better choice for irrigation channel leak detection.

The journal article “Water Stress Estimation in Vineyards from Aerial SWIR and Multispectral UAV Data” the authors detail how an UAV fitted with a multispectral camera (red, green, red edge and NIR bands) and a single band SWIR single band video sensor capable of recording in the 900 to 1700nm range can produce data that can be used to estimate the water stress in a vineyard. The UAV was flown between 80 and 100m height at a speed of 3m/s. This gave an 80% forward overlap and a side overlap of at least 80%. This is essential to produce continuous ortho-photo-mosaic images. The article does not say how the ortho-photo-mosaic images were made but later mentions the use of Agisoft Metashape Version 1.2 ®. It also does not mention how the Analysis Ready Multispectral SWIR data were produced. Calculation of spectral indices followed and canopy NDVI values were obtained. Problems were experienced in alignment of the ortho-photo-mosaic images but later versions (as used in this project) produce geo-referenced images. The next stage was to produce a scene reflectance dataset from the SWIR dataset. Applying the equation

$$\text{Leaf Area Index} = 4.9 \times \text{NDVI} - 0.46 \quad (\text{Johnson, 2003})$$

Overlaying the NDVI canopy map on the Leaf Area Index map will indicate, in this case, those vines that are not water stressed. This data could be used to identify potential leak sites in irrigation channels (Kandylakis et al., 2020). But the following factors need to be considered:

- a. The process is complicated and diverges from the need for real-time results in this project and,
- b. All the vegetation along the irrigation channel would need to be the same species and height so that an accurate Leaf Area Index could be calculated.

“Mapping Root-Zone Soil Moisture Using a Temperature–Vegetation Triangle Approach with an Unmanned Aerial System: Incorporating Surface Roughness from Structure from Motion” (Wang et al., 2018) details a project that is similar to the one conducted by Bian et al., 2019 (discussed previously). The methods of data collection are similar. Radiometric calibration of imaging sensors was required, together with geo-referencing of collected image data. A complex work flow was developed to generate NDVI values and land surface temperatures from the collected imagery. Then Agisoft PhotoScan ® (Agisoft LLC, 2018) was used to produce ortho-photo-mosaic images. The data from a spectro-radiometer was used to collect spectral radiance. All of the data was then used to produce a soil wetness index (SWI) map using the radiometric surface temperatures. Although a SWI was produced by this application in 2018 more up-to-date UAVs, cameras and processing software is now available. Therefore, it is felt that this project does not fit the role of a method to detect potential irrigation channel leakage sites with the accuracy, speed and cost-effectiveness required.

2.1.3 Estimation of Irrigation Channel Losses Due to Seepage

The paper titled “Estimation of seepage loss in irrigation canals of Tendaho sugar estate, Ethiopia” (Alamirew; Eshetu, 2018) used the inflow/outflow method to identify irrigation channel seepage losses. They calculated those losses were in the range of 3.26 MI and 4.6MI per km/day; with a mean value of 3.96MI. This is similar to the values advised by Goulburn Murray Water’s management as detailed in Paragraph 1.5.

2.1.4 Benefits of the Use of UAV in Agriculture

UAVs offer great benefits in detecting the leakage in irrigation channels as compared to traditional methods. Cruzan et al. (2016) discuss some of the advantages of using UAVs such as:

1. the collection of a large amount of quality data with minimal effort,
2. the ease of production of composite images (ortho-photo-mosaic images),
3. production of Digital Elevation Models (DEMs) and,
4. production of vegetation maps.

2.1.5 Other Uses for UAV

In recent years, UAV have become recognised as an excellent tool for crop management and have regularly been used in this role. Using the appropriate support software UAVs can determine over or under watering, irrigation scheduling, high or low chemical contents such as Nitrogen, Phosphorous and other trace elements (Sylvester et al., 2018).

The military is a leader in the practices of UAV (drone) surveillance or operational attacks. Other users such as Ergon Energy, a Queensland power distribution company uses UAV for power line inspections, repairs and even new construction in rugged terrain (Institute of Public Work Engineering Australasia, 2020). UAVs are ideal for monitoring areas that are inaccessible including broadcast radio towers. They give extremely high Ground Spatial Definitions (GSD) compared to commercial satellite imagery. Four cm per pixel GSDs are easily obtainable at flight height of 80m. This is an ideal height to avoid trees and power lines.

UAVs have been recently used for the remote sensing of wetlands (Baloloy et al., 2018) and this concept has been trialled for mapping aquatic vegetation in irrigation channels (Tiner et al., 2015).

2.1.6 Use of Green Normalized Difference Vegetation Index Compared with Other Radiometric Vegetation Indices

Gitelson et al (1996) write in the paper “Use of a Green Channel in Remote Sensing of Global Vegetation from EOS-MODIS”. A great amount of detail on how the use of the green channel in the reflectance spectrum relates to the amount of Chlorophyll-a (Chl-a). Although the paper discussed the data from the EOS-MODIS satellite in 1995 the data is relative to all imaging whether high-altitude satellite or low-altitude UAV images. They found that the maximum sensitivity of Chl-a was detected around the green band from 520nm to 630nm and near 700nm. Chl-a values between 0.3-45µg/cm² were identified in this range. This led to the development of the Green Normalized Difference Vegetation Index (GNDVI). This

Ch1 P6

$$GNDVI = \frac{(NIR - Green)}{(NIR + Green)} \quad (1)$$

In this project the ‘greenness’ index is required as there is a relationship between “greenness” and the amount of water leaking from the irrigation channel. Although this paper is now 24 years old the development of the GNDVI index is still appropriate.

The use of GNDVI is confirmed in the paper on “Broadband Greenness” (Harris Geospatial Systems, 2018). The GNDVI is more sensitive to Chl-a concentrations than the radiometric vegetation index Normalized Difference Vegetation Index (NDVI) and the GNDVI is also less sensitive to reflectance from soil.

The paper on “Applying High-Resolution Visible Channel Aerial Scan of Crop Canopy to Precision Irrigation Management” (Chen et al., 2018), states that they investigated multiple vegetation indices and found that while a majority of these indices use the relationship between red light bands and near-infrared band the red wavelengths are strongly absorbed by Chlorophyll and are less sensitive to alterations in the Chlorophyll content. They added that the green wavelengths are more sensitive to high Chlorophyll a and b levels. They also referred to the work of Gitelson et al., 1996, above, and confirmed that the GNDVI was the best index for measuring plant Chl-a. It should also be noted that the Index Database search for Vegetation Indices lists fifty Vegetation Radiometric Indices (Henrich & Bruser, 2022).

Further work by Gitelson and Merzlyak using a Hitachi 150-20 spectrophotometer confirmed that the GNDVI index was more sensitive to the Chl-a in a wide range of plant types than the previously used Normalised Difference Vegetation Index (NDVI). They estimate that the error was less than 2 nmol/cm² (Gitelson & Merzlyak, 1998).

2.1.7 Comparison of Vegetation Indices.

A summary of the most common used vegetation indices is shown as Table 1, below (European Space Agency, 2021 and Sykas, 2022). From Table 1, it can be seen that only the Green Normalized Difference Vegetation Index (GNDVI), Soil Adjusted

Vegetation Index (SAVI), Normalized Difference Vegetation Index (NDVI), Transformed Soil Vegetation Index (TSVI) and the Difference Vegetation Index (DVI) are relative to Chl-a detection. The work of authors in Section 2.1.6 above confirms that the GNDVI is the preferred Vegetation Radiometric Index for this project.

Table 1*List of Common Vegetation Indices*

Short Name	Name	Role
SAVI	Soil Adjusted Vegetation Index	More sensitive to Atmospheric variations than NDVI
NDVI	Normalized Difference Vegetation Index	Measures photosynthetic activity. Relates to density of vegetation
TSAVI	Transformed Soil Adjusted Vegetation Index	Measures slope and intercept of the soil line
MSAVI	Modified Soil Adjusted Vegetation Index	Applies correction factor to TSAVI
MSAVI2	Second Modified Soil Adjusted Vegetation Index	Reduces soil noise. Less sensitive than NDVI
DVI	Difference vegetation index	Sensitive to amount of vegetation
RVI	Ratio Vegetation Index	Indicates amount of vegetation. Reduces effect of atmosphere.
PVI	Perpendicular Vegetation Index	Generalization of DVI
IPVI	Infrared Perpendicular Vegetation Index	Functionally equivalent to NDVI
WDVI	Weighted Difference Vegetation Index	Mathematically simpler version of PVI
TNDVI	Transformed Normal Difference Vegetation Index	Indicates relationship between amount of green biomass in a pixel
GNDVI	Green Normalized Difference Vegetation Index	More sensitive than NDVI. Detects different concentrations of chlorophyll
GEMI	Global Environmental Monitoring Index	Designed to eliminate atmospheric correction.
ARVI	Atmospherically Resistant Vegetation Index	Related to atmospheric opacity.
NDI45	Normalized Difference Index	More linear equation than NDVI.
MTCI	Merris Terrestrial Chlorophyll Index	Estimates Chlorophyll from MERIS Imaging spectrometer.
MCARI	Modified Chlorophyll Absorption Ratio Index	Responsive to leaf chlorophyll and ground reflectance.
REIP	Red-edge Inflection Point Index	Measures nitrogen take-up in biomass.
S2REP	Sentinal -2 Red-edge Position Index	Interpolation of S-2 band 5 and 6. Red Edge
IRECI	Inverted Red-edge Chlorophyll Index	Estimates canopy Chlorophyll content.
PSSRa	Pigment Specific Simple Ratio Index	Evaluates range of pigments of the whole plant canopy.

Note: Source - (European Space Agency, 2021 and Sykas, 2022)

2.1.8 Relationship Between GNDVI Values and Chl-a Values

The GNDVI values are determined by the reflectance values in the green (500-600nm) and near infrared (750-950nm) bands (Artiola et al., 2004, pp183-206). Sonobe and Wang (2017) determined that a strong relationship between differential vegetation indices and Chl-a content. They found that the R^2 value (the proportion of variance) is 0.807 and the p value (probability) is <0.001. Where the p value (McLeod, 2019) is less than 0.1% then there is enough evidence to reject the null hypothesis (Corporate Financial Institute, 2021).

This indicates that there is a positive relationship between GNDVI and Chl-a values. Therefore, GNDVI can be used as a strong indicator of Chl-a values (Sonobe & Wang, 2017). A similar relationship was concluded by Tong and He in their journal article “Estimating and mapping chlorophyll content for a heterogeneous grassland: Comparing prediction power of a suite of vegetation indices across scales between years” (Tong & He, 2017).

Using this relationship, where high GNDVI values are found then high Chl-a values are identified and this indicates that the plant is receiving more than adequate nutrition and water. These high Chl-a values then imply that a location with a high GNDVI reading has plants that are receiving more water than the adjoining plants and suggests that this may be the location of a potential irrigation channel leak.

2.2 Current Methods of Leak Detection

The current methods of irrigation channel leak detection are:

1. When grass slashing occurs along the irrigation channel banks and leaks are identified,
or,

2. When water users complain to the irrigation channel management authority that a leak is water logging their crops,
3. During regular irrigation channel maintenance.

Currently, UAV do not appear to be used for irrigation channel leak detection in Australia. This lack of use of UAV may be caused by lack of familiarity with UAV and the results obtainable from their use and or the lack of Civil Aviation Safety Authority (CASA) licenced operators with the necessary equipment in their region.

2.2.1 UAV can Produce Better Results than Images from a Satellite

Satellites fly between a minimum of 600 and 36,000km elevation. High resolution images from these satellites may have a pixel size of 30cm per pixel. Higher resolution images may be purchased but as the size per pixel decreases the cost of the image rises inversely. Images from the GeoEye-1 satellite cost \$2750 for a minimum of 10,000 hectares with a multi-spectral resolution of 1.84m/pixel (Sozzi et al., 2018).

Ruwaimana et al. (2018) wrote their paper titled “The advantage of using drones over space borne imagery in the mapping of mangrove forests” where the authors conclude that the drone aerial photos provided higher quality images and was proven to be a viable alternative to satellite-based monitoring

Low level flights (30m to 100m), using an UAV produce photographs with a GSD of four cm and provide much finer detail at much lower cost. Specific areas can also be defined using a UAV where a purchased satellite image may cover a regional area of 25km x 23km (European Space Agency, 2015). By using a UAV, it will eliminate the need to correct imagery for

atmospheric distortion and clouds do not interfere with image collection. An UAV will provide a much smaller area of coverage than satellite images but the GSD will be much higher.

Images from an UAV flight can be checked as soon as the data is downloaded from the UAV memory card. If the UAV flight photography has any defects in the mission photography the flight can be re-flown immediately and at low cost. If clouds cover the area of interest on a satellite image it may be up to sixteen days before the desired satellite flies along the chosen path (United States Geological Survey, 2021). During the UAV flight the operator has a Visual Line of Sight of the UAV's position in relation to the ground and can adjust this if necessary. The flight times can be chosen so that major reflection off the contained water in the irrigation channel and tree shadows are not a problem. The preferable times are between 1000hrs and 1400hrs to eliminate reflection off the irrigation channel water and shadows from nearby trees (Sylvester et al., 2018).

The journal article on the "Assessment of Aquatic Weed in Irrigation Channels using UAV and Satellite Imagery" (Brinkhoff, Hornbuckle, and Barton, 2018) contains specific information from the UAV aspect, has a great amount of information relative to this project. Details such as the methods of differentiating between aquatic and natural vegetation, the interference from reflectance values of the channel water, supervised and unsupervised classification of results, the use of multi-spectral cameras and high resolution (GSD of 5cm) images. A comparison between satellite and UAV effectiveness shows that the UAV produced better, quicker, cloud- free and cheaper results than 30cm pan-sharpened satellite images. The methodology of using a multi-spectral camera eliminated the time-consuming need to match separate images of the same location.

2.2.2 Use of Infra-red Imaging

A different method of detection of irrigation channel leakage hotspots is the use of thermal infrared imaging. Thermal infrared imaging will only detect the temperature differences at locations along the irrigation channel. It will not detect the presence of moisture in the irrigation channel banks (Price, 1980). Also, the use of thermal infrared imaging will only detect temperature variations in the top few millimetres of the soil surface (Carlson & Petropoulos, 2019).

A method of detecting and estimating soil moisture (M_o) values is the use of a simplified triangle that utilises the NDVI index value plus the surface radiometric temperature (T_{ir}). The data collection can be either by orbital satellite or UAV fitted with a thermal imaging camera (Carlson & Petropoulos, 2019). The DJI P4 UAV used in this project has the ability to have a thermal infra-red camera fitted as an option.

To process the data, it is necessary to create a Fractional Vegetation Cover (F_r) using the formula:

$$F_r = ((NDVI - NDVI_o) / (NDVI_s - NDVI_o))^2 \quad (4)$$

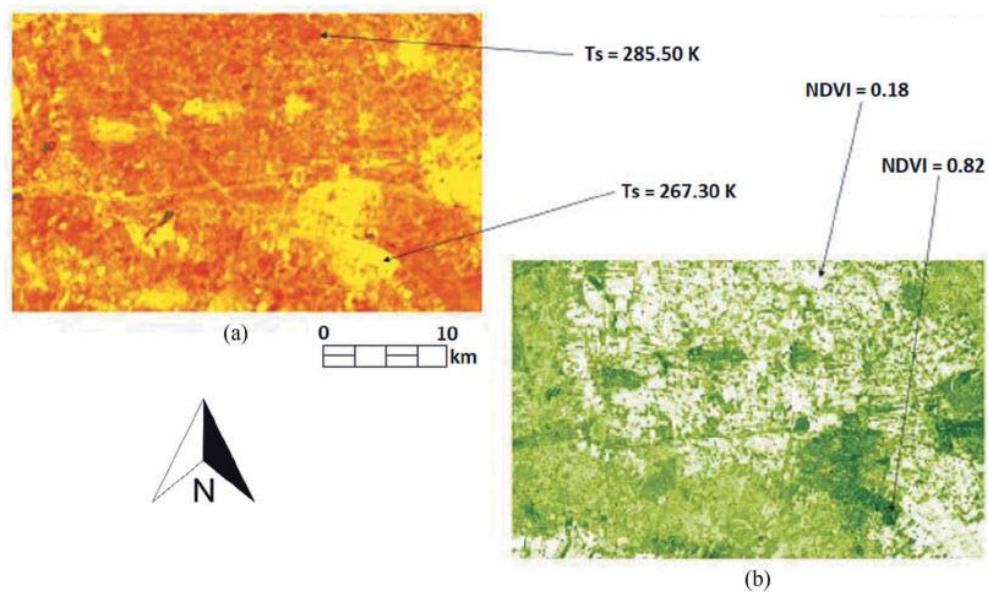
Where $NDVI_o$ is the value of the bare soil, $NDVI_s$ is the value of the green patch. Next a Scaled Infrared Surface Temperature (T^*) is prepared using the formula:

$$T^* = (T_{ir} - T_{min}) / (T_{max} - T_{min}) \quad (5)$$

Where T_{min} is the temperature of the green cover and T_{max} is the temperature of bare soil. Figure 12 explains this.

Figure 12

Thermal Infra-red image and NDVI image.

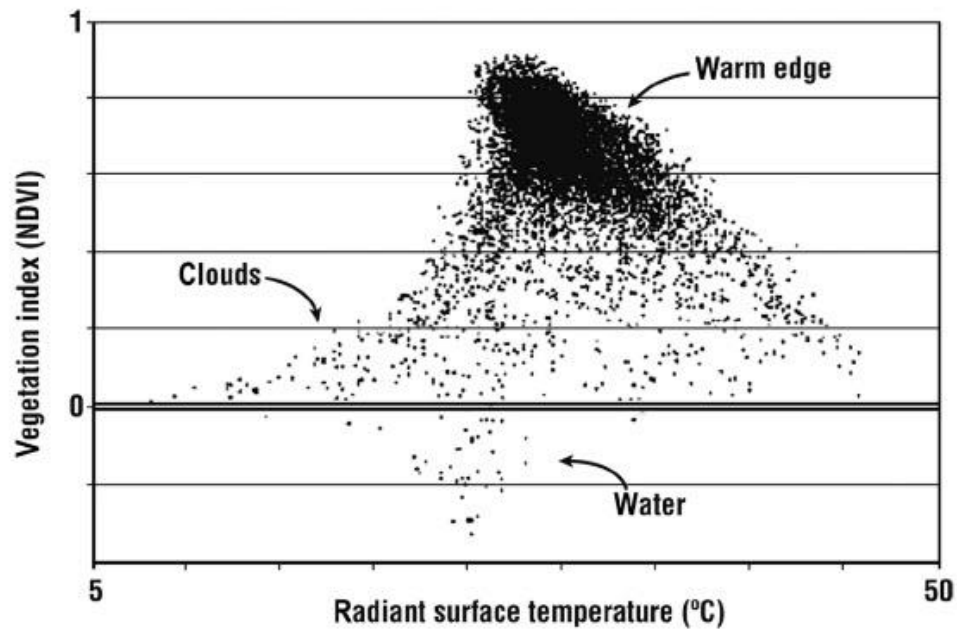


Note: Source - Carlson & Petropoulos and Gillies et al (Carlson & Petropoulos, 2019 and Gillies et al.,1997).

The values of F_r and T^* are then plotted on a two-dimensional triangle to determine if soil moisture is present. Figure 13 below is an example of this type of plot.

Figure 13

Two-dimensional tri-angle plot.



Note: Source: (Carlson & Petropoulos, 2019).

However, this system has the following problems:

1. Requires thermal infra-red images and optical images of both bare and vegetated soil,
2. Adjacent dissimilar vegetation may give incorrect readings,
3. Difficult to interpret results if standing water is present and
4. Results are not geo-referenced.

3 CHAPTER 3: DATA and METHODOLOGY

3.1 Introduction

This chapter will discuss aspects of the of preparation for the UAV Flights, identifying the software needed to produce the ortho-photo-mosaics and the application to calculate the GNDVI values and then to produce a map showing the geo-referenced potential irrigation channel leakage sites.

3.2 Pre-flight Preparation.

3.2.1 Software Identification and Installation

The European Space Agency SNAP toolkit (European Space Agency, 2021) and Agisoft Metashape® Pro (Agisoft LLC, 2021) were installed on to a Lenovo Idea-pad 110 Laptop computer for processing of the data downloaded from the UAV via SD memory card. Global Mapper V24 (Blue Marble Geographics, 2020) was also installed for the final production of the potential irrigation channel leak hotspots.

3.2.2 UAV DETAILS.

The UAV chosen for this project was a P4 UAV from Di-Jiang Innovations (DJI) of Shenzhen, China. DJI now hold up to 70% of the UAV market for both commercial and leisure aircraft (Spires, 2021). The UAV used in this project is fitted with a multispectral camera and is shown below in Figure 14 (DJI Industries Limited, 2021). This UAV can fly for 30 minutes on one battery, is resistant to wind turbulence and is a stable platform for high grade image collection.

Figure 14

DJI P4 UAV with multi-spectral camera.



Note : Image source : DJI Industries (DJI Industries Limited, 2021).

The camera is fitted with the following complementary metal oxide semiconductor (CMOS) sensors as per Table 2 below. This data is from DJI Multi-spectral camera specifications (DJI, 2021).

Table 2.

Properties of DJI P4 UAV Multi-spectral camera.

Band	Wavelength(nm)	Remarks
Blue	450 +/-16nm	Not used in this project
Green	560 +/-16nm	Required for GNDVI
Red	650 +/-16nm	Not used in this project
Red Edge	730 +/-16nm	¹ See below
Near-Infra Red	840 +/-26nm	Required for GNDVI
RGB Sensor	Multiple	Visible light Imaging

Note : Source : DJI Industries (DJI Industries Limited, 2021).

3.2.3 Radio-metric Calibration of DJI P4 4 UAV.

Radio-metric calibration takes into account the atmospheric and solar conditions present and converts them into a digital index of scene reflectance that is used in quantitative remote sensing. This data may differ from every image taken. This data is also used in the calculation of vegetation indices. Consequently, a standard procedure for the system of radio-metric calibration is necessary using a linear regression method (Guo et al., 2019).

For this project the radio-metric calibration of each image is calculated in the post-processing stage using Agisoft Metashape Pro ® software (Agisoft LLC, 2021).

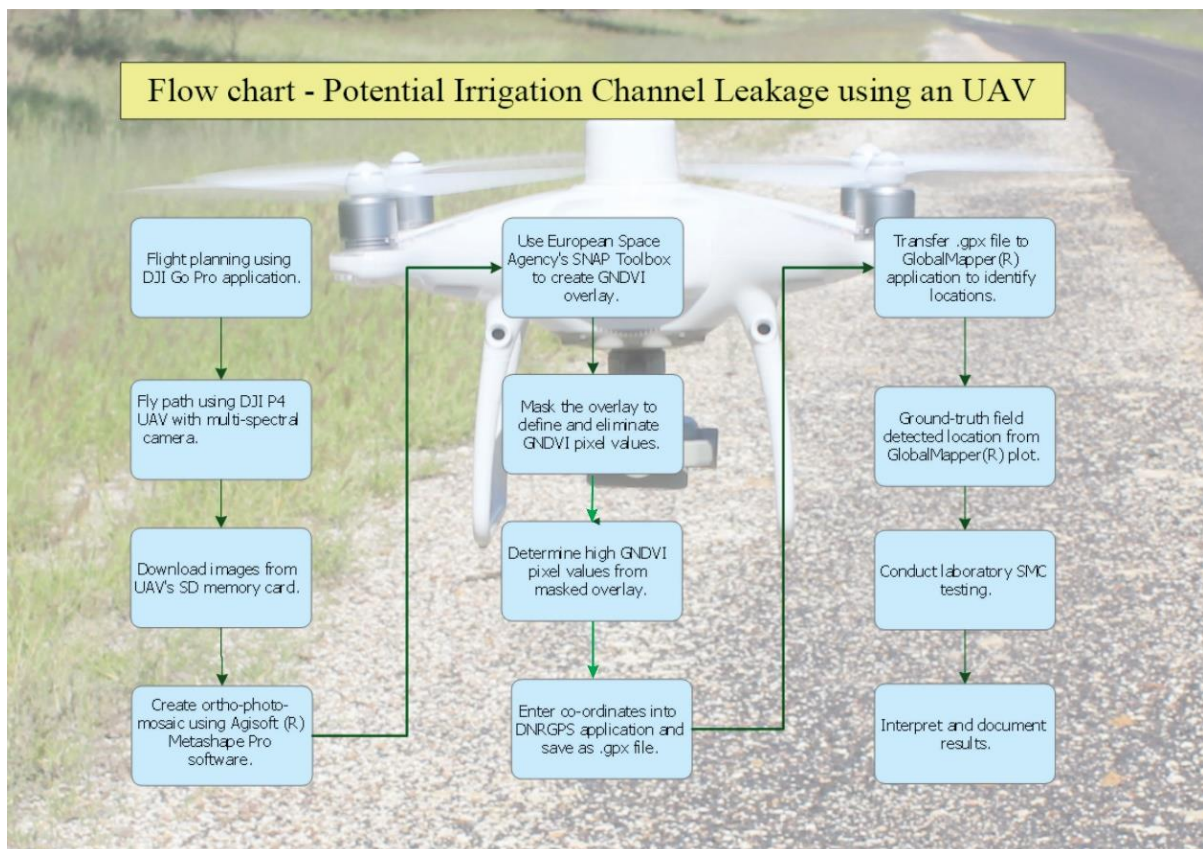
¹ The red edge band is better than NDVI for the early detection of plant disease. Not used in this project.

3.2.4 Flow Chart for the Process of Irrigation Channel Leak Detection

Figure 15 below is a flow chart of the process of using an UAV for the detection of potential irrigation channel leaks.

Figure 15

Flow chart of process of identifying potential irrigation channel leaks.



3.2.5 Pre-flight Planning

Flight planning for the DJI P4 UAV is done with the use of DJI GS Pro (Ground Station Pro) Flight Management software (DJI Technology Co., Limited, 2022). This software is commercial and is sold on a month-by-month fee payment basis. Table 3 below shows the properties that can be used in this software. The data in this table comes the meta-data of images from Flight Path #1 at St George on 12 April 2022.

Table 3

Flight data for DJI P4 UAV

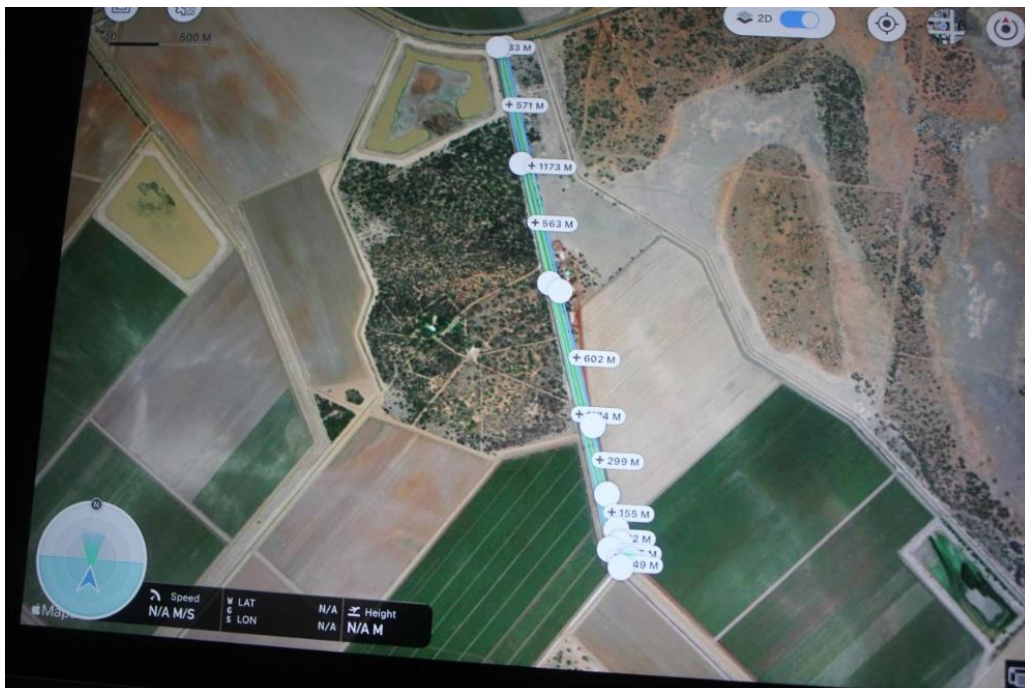
Speed	Height	GSD	Forward Overlap	Lateral Overlap
3.8 m/sec	55m	2.9 cm/pixel	80%	25%

Note : Source : DJI Industries (DJI Industries Limited, 2021).

The flight plan for Flight Path #1 on the Bundoran Road B2 channel is shown as Figure 16 below. The numbers along the flight path are waypoints that create a change of direction for the UAV. The flight parameters for the UAV such as flight height and speed are pre-set-set before the flight commences.

Figure 16.

Screen capture of DJI GS Pro Flight Plan # 1.



Note: Source - DJI GS Pro (DJI Technology Co., Limited, 2022). Own photograph.

The protocols for this flight have been developed using DJI's Software Development Kit (SDK) to control the aircraft's flight stabilization, signal transmission and communication. To this SDK is added the actual flight details such as waypoints using location co-ordinates, mission heights, when to start and stop the cameras, lateral and forward overlaps for photographic images, return to home altitudes and flight speed.

All of this data is transferred to the UAV via a protocol called Micro Air Vehicle Link (MAVLink) (DroneCode Inc, 2020), a protocol designed for use by UAVs. It allows for combinations of flight plans and instructions related to aerial photography to be adopted in the sequence directed by the flight originator. For example, instructions such as Take off - Reach planned mission height - Commence taking images - Go to consecutive waypoints – Return to home – Stop taking images – Land – Shutdown.

MAVLink instructions are sent to the UAV using a File Transfer Protocol (FTP) and are transmitted from the remote controller using the Wireless Fidelity (WIFI) system that is an integral component of the UAV.

3.2.6 Satellites required by the UAV

The DJI P4 UAV requires a minimum of six satellites to be locked into its navigation system before it will fly. The more the better as greater accuracy can be achieved. Global navigation system satellites provide the UAV with data to:

1. identify and return precisely to the home station where the flight began,
2. help keep the UAV stable when in flight,
3. keep the UAV at the nominated level above ground level,
4. identify the UAV's position continuously on the map on the control tablet,

5. allows the plotting of flights using waypoints and keeping the UAV on these plotted waypoints and,
6. in the event of a control disaster assist in finding a crashed or missing UAV.

3.2.7 Global Navigation Systems Used to Control the UAV

Four Global Navigation Satellite systems (GNSS) were available and used by the DJI P4 UAV; depending on which satellite was overhead. These systems are the Global Positioning System owned by the US, BeiDou of Chinese origin, Galileo launched by the European Space Agency and Glonass of Russian origin. The precision of the GNSS data was improved using Real-Time Kinematic (RTK) positioning using built in wireless connection to the nearest Continuously Operating Reference Station (CORS) station.

3.2.8 Proposed UAV Flight Parameters

It was decided to fly the UAV between 50 and 80 meters above ground level to avoid trees and high voltage power-lines in accordance with the risk assessment conducted prior to the flight. Flights are planned to be started in the middle of each flight path so as to obtain the maximum 'line of sight' for each flight path. Each flight commences in the centre of the individual flight path, flown to one end and then to the other. Starting in this manner provides two passes over each flight section of the irrigation channel and helps produce a more comprehensive ortho-photo-mosaic when the image data is processed. Flying twice along the irrigation channel allows maximum coverage of the irrigation channel while keeping the UAV under visual control as required by CASA's Flight Rules (Civil Aviation Safety Authority, 2019).

3.2.9 Field Checking of Downloaded Data from UAV.

Images from the UAV are available as soon as the UAV lands. The image data can be downloaded from the UAV's memory card and checked for clarity, site accuracy and completeness. If any of these problems are evident the flight can be re-flown immediately. Doing this on location in the field allows for a check of the quality and quantity of the downloaded images prior to the preparation of the ortho-photo-mosaic image of the potential leak sites on a larger and more powerful PC.

3.2.10 Production of the Ortho-Photo-Mosaic.

Agisoft Metashape® Pro is a software package that undertakes photogrammetric processing of digital images. These images can come from low altitude UAV photographs, normal aerial photography or satellite images. This package can use imagery used in Geographical Information Systems (GIS) such as Geotiffs or georeferenced .jpg file packages to produce ortho-photo-mosaic images. Using data or images from a multispectral camera on-board a UAV the software can produce dense point clouds, textured polygonal models, digital elevation models (DEM) and geo-referenced ortho-photo-mosaic images. It is capable of processing 50,000 images for each project. (Agisoft LLC, 2021). An ortho-photo-mosaic is the result of joining the collection of individual photographs from the capturing camera. The ortho-photo-mosaic is produced in the following sequence:

1. Align the photos by searching for feature points on each image and matches them using tie points. The program also looks at the image to find the position of the camera and estimates the camera calibration parameters. This is done by:
 - a. detecting similar points in each photo,
 - b. selecting pairs,

- c. matching identified points,
 - d. estimating camera locations.
2. Generation of a surface 2.5-dimension Digital Elevation Model (DEM). The 2.5D DEM is defined as a “*Digital elevation model (DEM) is a 2.5D model of a surface represented in a form of a regular grid, with height values stored per every cell of the grid*” (Agisoft LLC, 2021, pp 46-47).
 3. This section of the software process relates to the production of the DEM. In this process the images are converted into a 2.5D model which shows both the terrain and all objects above the ground such as natural and artificial features. This is a photo-realistic representation of the flight path flown. This preserves the original resolution of the images.
 4. Building the ortho-photo-mosaic using the DEM is completed by projecting the images onto either a mesh or 2D images in a manner determined by the camera internal or external orientation parameters. At the same time the ortho-photo-mosaic is georeferenced, using the Metadata contained in each image. An example of the completed ortho-photo-mosaic for Flight Path # 4, flown on 9 April 2021 is shown below as Figure 17, where under magnification, minute details are clearly visible (Agisoft LLC, 2021).

Figure 17

Ortho-photo-mosaic of UAV Flight with enlarged vehicles.



Note: Source – Processing from Agisoft Metashape® Pro (Agisoft LLC, 2021).

3.2.11 Components of the Ortho-Photo-Mosaic Image

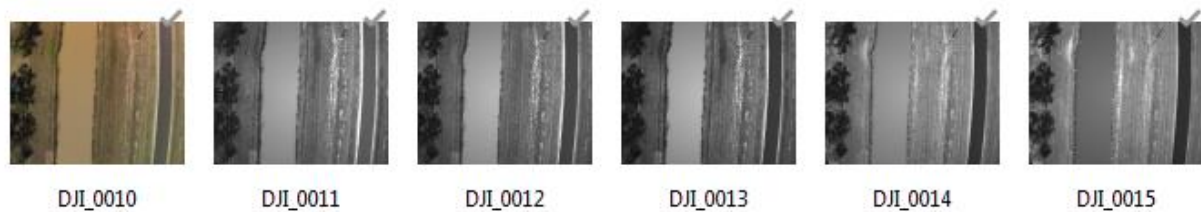
The ortho-photo mosaic images are exported as Geo-tiff or georeferenced .jpg files for further processing. The next stage is to open the ortho-photo-mosaic in the European Space Agency's SNAP toolkit (European Space Agency, 2021).

In this project the post processing includes creation of the GNDVI overlay and developing masks to indicate the high Chl-a plants along each flight path.

Each individual image from the P4 UAV comes geo-referenced. When the ortho-photo-mosaic is produced it is also fully geo-referenced. Previous use of the Agisoft Metashape® software suggests that the production of each ortho-photo-mosaic can take up to one hour and thirty minutes for a twenty-minute UAV flight. Each image set contains a red, green, blue, near infrared, red edge and red-green-blue composite images, taken collectively at the same time. Figure 17 shows these images from Flight Path #1, flown on 9 April 2021.

Figure 18

Image set from DJI P4 multi-spectral camera.



Note: From left RGB, red, green, blue, red edge and near Infra-red image bands.

Source: Processing from Agisoft Metashape® Pro (Agisoft LLC, 2021).

3.2.12 Processing the Ortho-Photo-Mosaic Using the European Space Agency's SNAP Toolkit

The SNAP Toolboxes from the European Space Agency include twenty-one Vegetation Radiometric Indices. Although these Toolboxes are developed and maintained for the use of satellite images, they work perfectly on ortho-photo-mosaic images from UAVs. The ability to produce the GNDVI image is a built-in function of the SNAP toolbox. All that is required is to load the ortho-photo-mosaic image into the software and select the GNDVI Processor from the available Vegetation Radiometric Indices. After setting the processing parameters and identifying the green source band and the Near Infra-Red (NIR) source band the software will

then produce a new file with GNDVI in the filename. The next stage in the process is to place a mask over the GNDVI image to identify the high Chl-a hotspots (Braun, 2021).

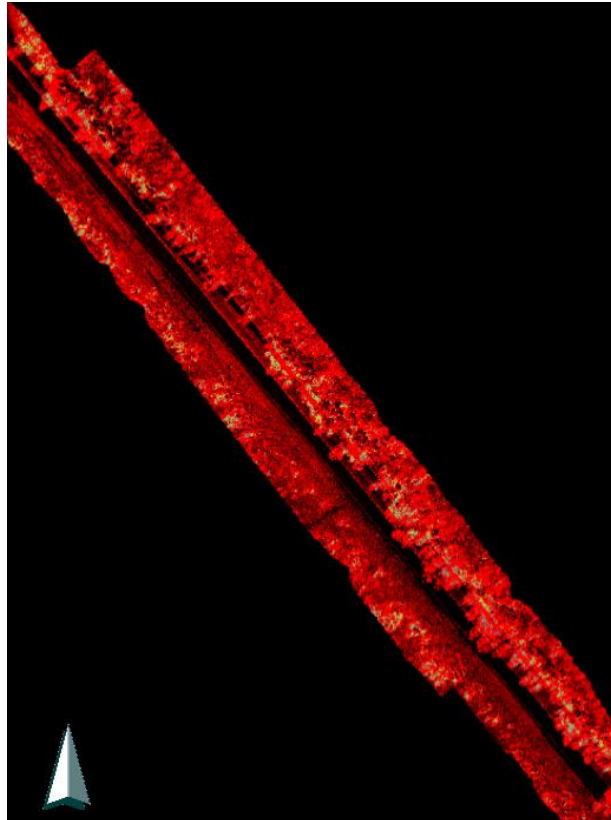
3.3 Mask overlays

3.3.1 Use of High Chlorophyll-a mask

The SNAP Toolbox makes provision to overlay the GNDVI image with a mask to identify the Chl-a hotspots. The Mask Manager included in the software provides the ability to use logic or mathematic expressions on the pixels of an image to identify which pixels meet the stipulated conditions. It also includes the systematic analysis of the spectral response of particular surfaces using criteria from both the optical and microwave spectrum. This allows for precise determination of specific surfaces (Braun, 2021). Figure 19 below shows the use of the mask manager with GNDVI setting of between 0.80 and 1.0. In this example the mask is duplicated using both yellow and blue colours to increase the visibility of the hotspot locations. The yellow hotspots to the right of the irrigation channel are trees with a high Chl-a value.

Figure 19

Mask Manager set for between 0.8 and 1.0 GNDVI and resulting hotspot map



Note: Hotspot Transparency set $0.8 < 1.0$. From European Space Agency SNAP Toolkit (European Space Agency, 2021).

Only locations identified as hotspots near the banks of the irrigation channel are considered to be potential irrigation channel leaks. This is seen in the above image where yellow hotspots appear on the left and right edges of the image and may not be irrigation channel leak but vegetation with high Chl-a values.

Figure 20 is an image is from Agisoft Metashape® Pro V1.7.2 and the ESA SNAP Toolbox V7.9 and shows the GNDVI overlay in red. Subsequent versions of each software only show the GNDVI overlay as gray. Mask colours can be chosen from a range of 13 basic colours.

Figure 20

GNDVI image derived from ortho-photo-mosaic.



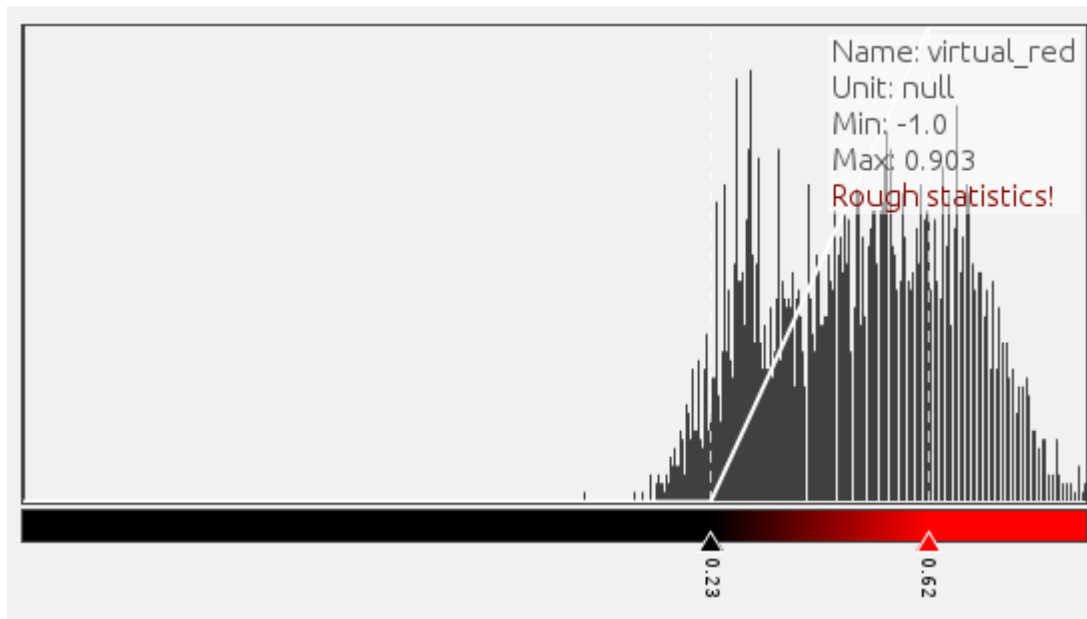
Note: From European Space Agency SNAP Toolkit (European Space Agency, 2021).

The red values in Figure 20 above are graded colour depending on the calculated GNDVI results (from -1 to +1) from the SNAP Toolbox Vegetation Radiometric Index calculation. The histogram of the colour strength, which relates to the value of the GNDVI is shown below as Figure 19. Using colour manipulation properties of this histogram the values of the GNDVI and consequently its represented colour, can be increased or decreased. If increased, it will show a deeper red colour for the higher GNDVI value. The red value is set to 0.62 which is the value used in Figure 17 above.

The data in the GNDVI can be further evaluated using a Mask to generate the high Chl-a values which lead to detection of potential irrigation channel leakage sites.

Figure 21

Colour manipulation histogram

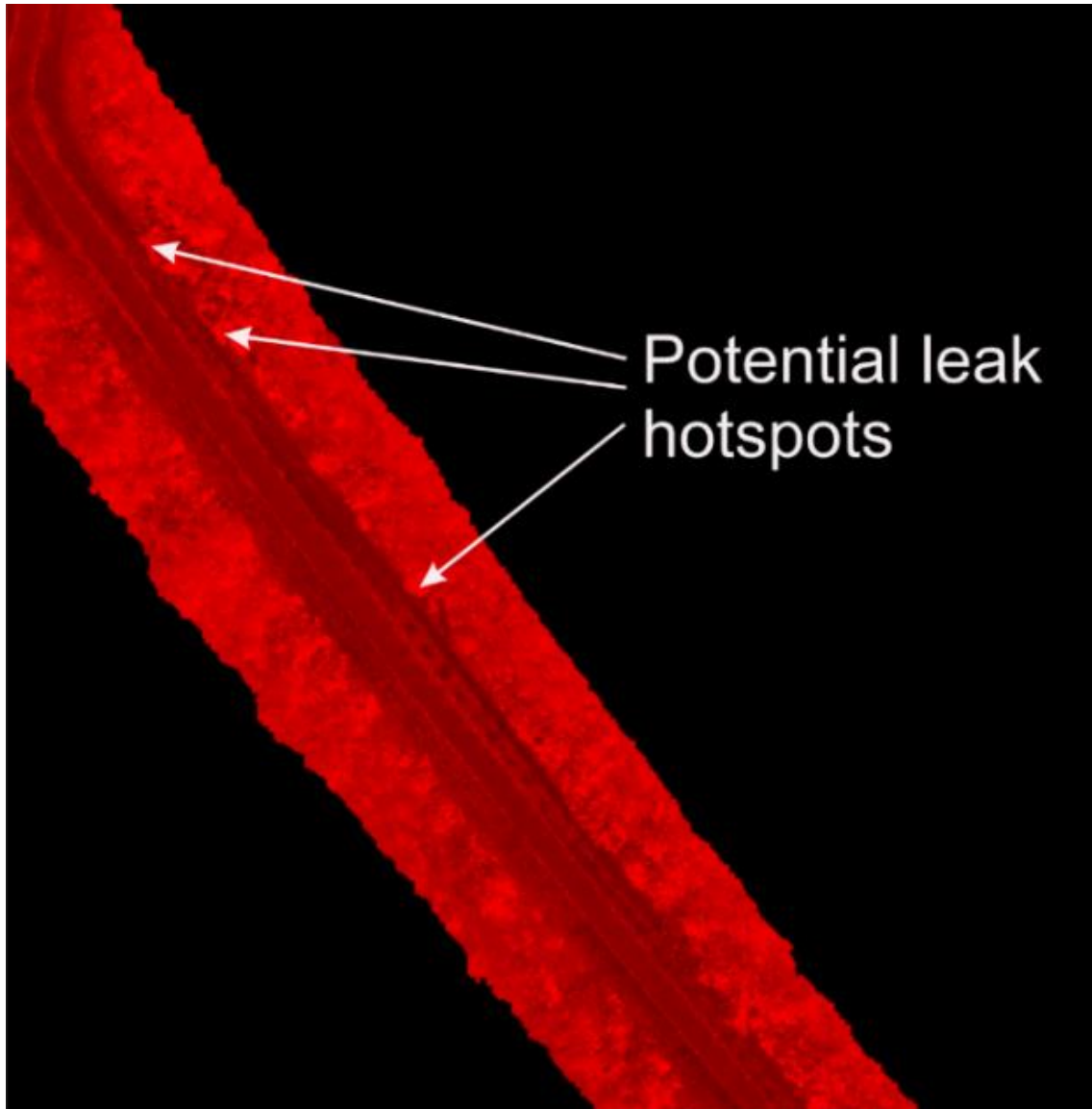


Note: From European Space Agency SNAP Toolkit (European Space Agency, 2021).

Figure 22 shows the same image as Figure 20, above, but with the black value decreased to 0.41 and the red value increased to 0.84. By doing these alterations the potential hotspots are visible.

Figure 22

Manipulated colours of GNDVI overlay



Note: From European Space Agency SNAP Toolkit (European Space Agency, 2021).

3.4 Creating the GNDVI Hotspot Maps and Confirmation of Hotspots

3.4.1 Preparation of Hotspot Location Map.

The locations of the interpreted hotspot are transferred to a Geo-referenced map of the flight locations. This is performed using the Minnesota Department of Natural Resources DNRGPS © software (Minnesota Dept of Natural Resources, 2021). Similar to an Excel ® spreadsheet but it has the ability to save the co-ordinates as a .gpx file which is easily transferred as an overlay to the Geographical Information System software, Global Mapper® from Blue Marble Geographics Inc of Maine, USA (Blue Marble Geographics Inc, 2021). This application is similar to ArcGIS® or QGIS® but is more user friendly.

3.4.2 Confirmation of Leakage Hotspots.

When the locations of the hotspots have been identified it will be necessary to prove that the hotspot location is an actual irrigation channel leak or a false positive reading. A false positive reading may be an indication of a high Chl-a plant in the vicinity. An example is shown in Figure 40 where high Chl-a vegetation in the form of a Cactus has been identified close to the irrigation channel bank. False negative locations may also be identified by visual inspection. A false negative value was encountered in April, 2022. In this circumstance deep vehicle ruts along Flight Path 4 suggested that leaking was occurring in the irrigation channel bank but the location was not recorded as a hotspot on the GNDVI map. False positives and false negatives can be confirmed by taking a soil sample at an appropriate depth in the vicinity of the irrigation channel bank and testing the Soil Moisture Content (SMC) to see if this is above the base value. The base value can be determined by taking a SMC sample from control points located

away from the irrigation channel and not under any influence of that channel or any subsequent irrigation.

3.4.3 Ground Truthing Control Holes

Control holes, similar to the holes used in the ground-truthing procedure, will be dug away from the influence of any leakage from the irrigation channel, or any irrigated pastures or crops, will be dug and their SMC recorded. Each flight path will have a control hole to provide a base SMC value. If variations in the soil types occur in the vicinity of these control holes, then additional holes will be dug in each variation of the soil type. The results from these control holes will be used for comparison of SMC samples from the ground- truthing holes along the irrigation channel banks.

3.4.4 Ground-truthing Procedure.

To confirm if the identified location is or is not a hotspot a 15 mm diameter hole will be drilled to a depth of one meter and a soil sample extracted for SMC testing. Three samples will be taken at each location. The first at the base of the irrigation channel wall. The second and third samples will each be taken at one-meter intervals along a transect line at right angles to the irrigation channel wall.

This will confirm if higher soil moisture contents are occurring; suggesting that the irrigation channel is leaking and allowing water to penetrate the surface (A horizon), the Subsoil (B horizon) or the Regolith (C horizon).

The SMC sample will be bagged in a tough foil lined paper bag and weighed on site. The soil sample will be eventually transported to the University of Southern Queensland (USQ) at Toowoomba and be oven dried at 110 degrees C for a minimum of 16 hours in USQ's soil

laboratory drying oven in accordance with Australian Standard AS1289 B1.1 (Standards Australia, 2022). The sample will then be re-weighed and the soil moisture content of the SMC calculated and recorded. After determining the SMC of the samples, they will be compared to the Munsell Soil Colour Classification Chart (Landa, 2004) to assist in recording of the soil colour. The Unified Soil Classification System (USC) Civil Engineering. (2019), will then be used to determine and record the classification of the soil type to see if soil types affect any irrigation channel leakage.

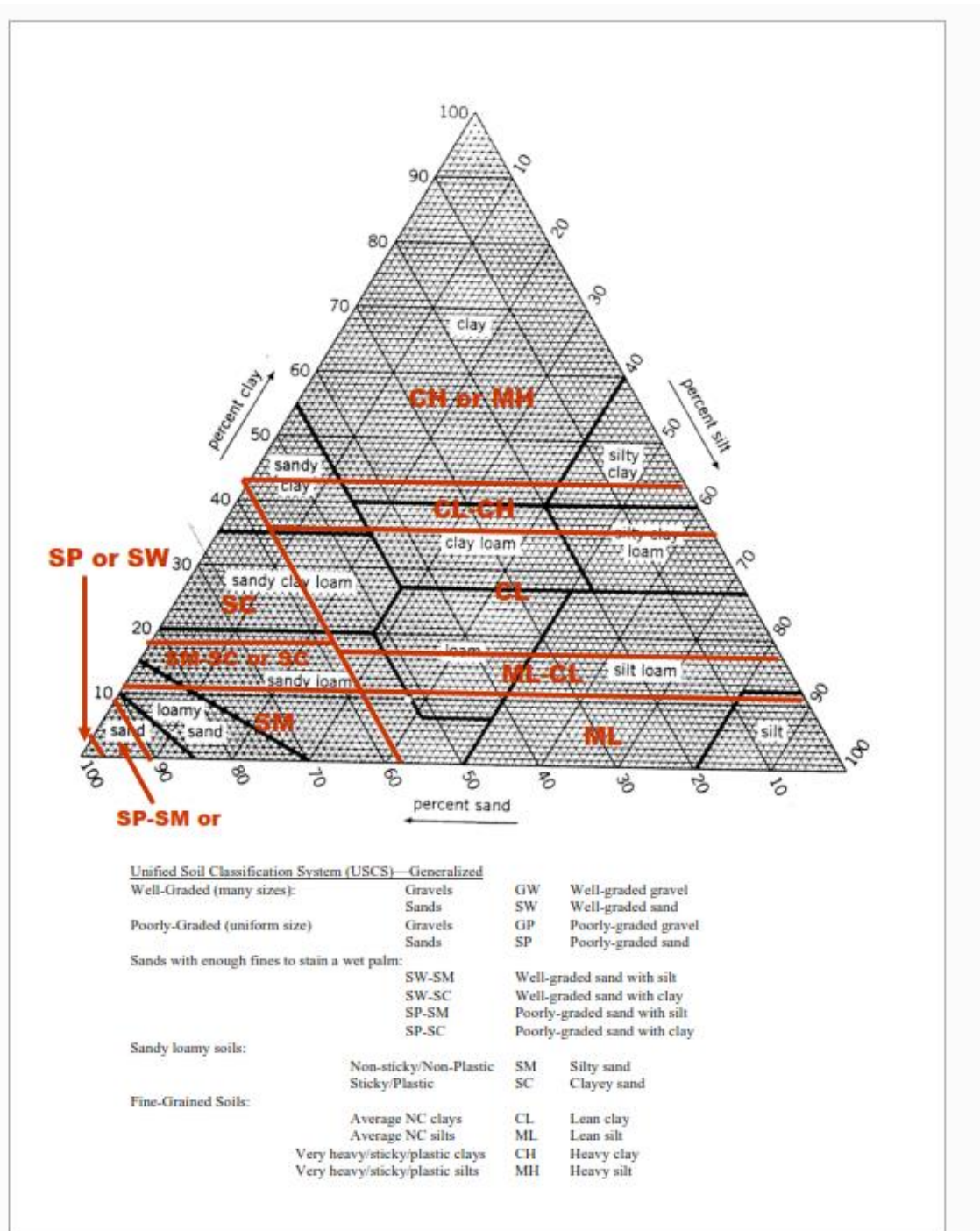
3.4.5 Unified Soil Classification System

The USC System was developed by A Casagrande (Wilson et al., 1982) for use on airfield construction in WW2. Modified during later years it has become the standard for soil classification other than for highways. It is now used world-wide (Civil Engineering, 2019). For highways in Australia² the American Association of State Highway Officials (AASHO) system is used (US Department of Transportation, 2017). The chart used in the Unified Soil Classification System is shown in Figure 23 below.

² Personal knowledge as a previous employee in the South Australian Highways Department Material Laboratory.

Figure 23

Unified Soil Classification System chart



Note: From- 'Civil Engineering' web page (Civil Engineering, 2019).

3.5 Other Considerations

3.5.1 Risk Assessment

For the St George region, a risk assessment is required to be done prior to UAV flights in accordance with USQ and Mallowa Irrigation Limited policies. This risk assessment will be conducted along the irrigation channels, B2, B2/2 and Munro Road. This risk assessment will look at factors such as tree height, power line height, residential and farm buildings and safe access to the banks of all lengths of the irrigation channels. In addition, other factors such as daytime heat, flies and sand-flies are to be considered.

3.5.2 Insurance and WH&S Equipment Provisions

Mallowa Irrigation Limited has a copy of USQ's public liability policy. Other insurances, such as loss or damage to the UAV are held by the UAV flight operator that either donated their services or were under contract to the University.

All personnel involved in this project will be required to wear the appropriate personal protection equipment as defined by Mallowa Irrigation Limited's WH&S policies.

3.5.3 Notification to Landowners of Proposed Flights

All landowners using irrigation water are to be notified in advance by email from Mallowa Irrigation Limited. This notification included the planned flight date, times, aircraft heights, expected noise levels and that no flying or photography would be conducted on private land but only on Mallowa Irrigation Limited's irrigation channel easements.

3.5.4 Aerial Crop Sprayers and Civilian Aircraft

The two aerial crop sprayers in St George, Precision Aerial Limited and Ballonne Airwork Pty Limited, are to be consulted on the morning of this project's proposed flight. Liaison with these companies is essential for the safe conduct of this project.

High Frequency (HF) radio communications is to be maintained with these aerial crop sprayers in the event that their operations may have a conflict with the flight operations planned for this project.

St George airport is uncontrolled but Regional Express (REX) Airlines serve this location. Good liaison is required to ensure that their flight operations do not interfere with the UAV flights (Airport Guide, 2021). All UAV flights will be conducted in accordance with CASA's flight safety rules.

4 CHAPTER 4: RESULTS and DISCUSSION

4.1 Introduction

This chapter will provide the results from UAV flights over the irrigation channels in St George in Western Queensland. These results are for the flights conducted on 9 April 2021, as Phase 1 and 12-13 April 2022 as Phase 2. The results will include problems experienced, how the UAV flights were conducted and their location, acquisition of photographic images, production of the ortho-photo-mosaics and the GNDVI masks. Mapping of the identified hotspots is then shown together with a table of the ground truthing results. This table includes the location, SMC recorded, Unified Soil Classification Class and the Munsell Soil Colours. This data will help in the determination if the potential hotspot is an actual or potential irrigation channel leak.

4.2 ST GEORGE – PHASE 1 – 9 APRIL 2021.

4.2.1 Factors Affecting the Possible Outcomes

First it is necessary to look at factors that may have influenced the result outcomes. They are shown below as rainfall, grass slashing, ground truthing hole depth, irrigation channel planned but not included in this project and risk assessment results.

4.2.1.1 Rainfall.

Between 1 Mar 2021 and 9 Apr 2021, 139.2mm of rain had fallen in the St George area (FarmOnLine Inc, 2021). This rainfall promoted a rapid growth of grasses such as Buffell Grass and Rhodes Grass (Qld Department of Agriculture, Forests and Fisheries, 2013). This growth is visible along the banks of irrigation channel B2, as shown in Figure 24 and Figure 25. It should be noted that Buffell Grass is not tolerant to high water levels in the soil (Cook, 2007).

The SMC values along Flight Path #4, where the photos in Figures 24 and 25 were taken were all below 1.16%. This indicates that high SMC values were not present. The Buffell Grass in Figure 24 is over 1m high confirms that high SMC values are not present along this part of the irrigation channel system.

Figure 24

Hotspot location 4.2 showing Buffell Grass on bank



Note: 9 Apr 2021. Irrigation channel is to the left of this image. Own photo.

Figure 25

Rhodes Grass near irrigation channel bank



Note: Source – Own photo 2021.

4.2.1.2 Grass Slashing.

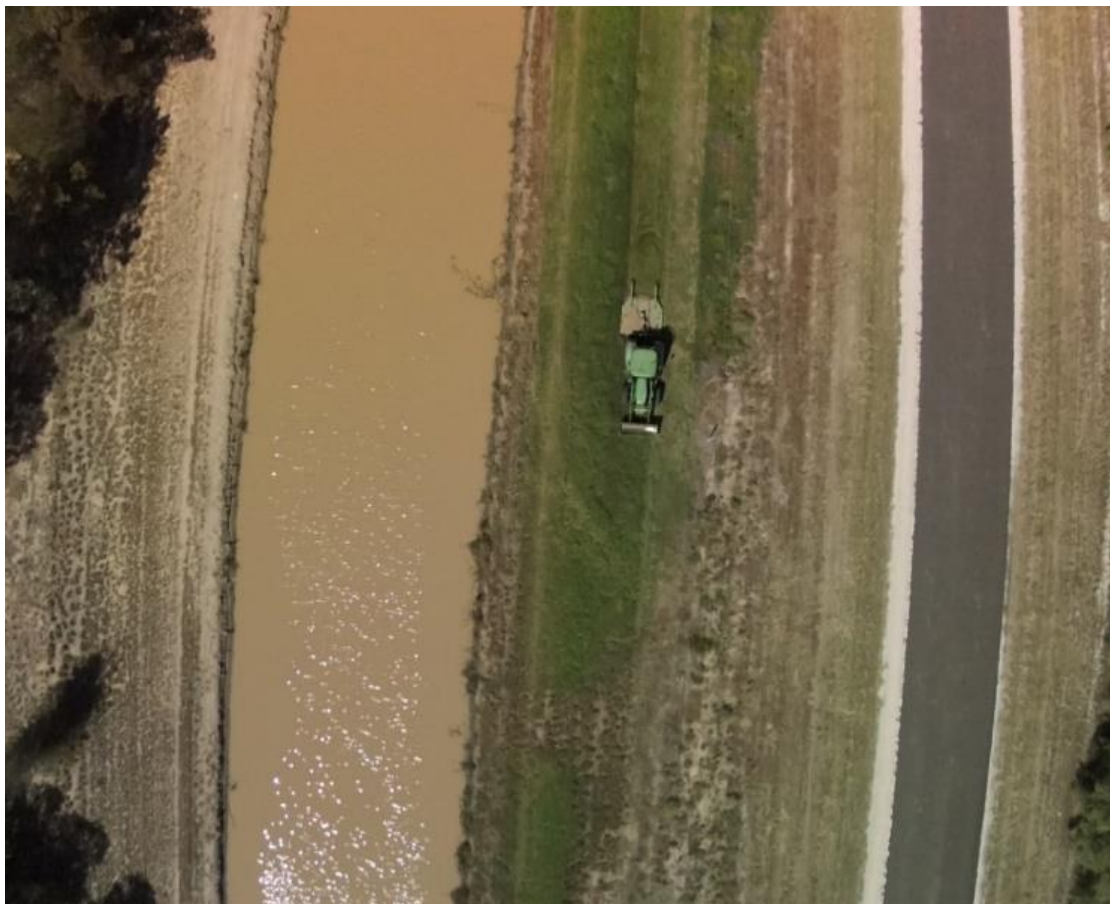
Grass slashing was in process along Flight Path #1 sector. Although this did not physically interfere with the UAV flight operations it may have interfered with the true value of hotspots detected. Some slashing had been done on previous days and the drying of the grass would have altered the Chl-a values compared to had it been left standing. This may have given a false-negative value to the GNDVI readings obtained.

However, during ground-truthing in the Flight Path #1 sector six hotspot locations from the GNDVI mask that covered this area were investigated. Because these hotspots were spread along his sector and values of these hotspots was low it is felt there was minimal interference

because of grass slashing. The grass slashing tractor is clearly visible in Figure 26, one of the many red-green-blue images from the multi-spectrum camera on board the DJI P4 4 UAV, below.

Figure 26

Grass slashing tractor from UAV Flight Path #1.



Note: From DJI P4 4 images, Flight Path #1, 9 Apr 2021.

4.2.1.3 Ground-truthing Hole Depth.

The low SMC of the soil at the base of the irrigation channels did not allow holes to be drilled, using a powered auger, deeper than 300 mm instead of the planned 1m. The hole depth of 1m

was based on most of the irrigation channel banks were approximately 2m high. Drilling the ground-truthing hole to 1m below the base of the irrigation channel wall would have given a “wetable” profile of at least 3m. The inability to drill this hole greater than 300mm due to the soil hardness was confirmation that leaking was not occurring at that location. This inability was caused by the hard nature of the drier soil at the A and B horizons. As the SMC value seemed to be continuous for the first 300 mm it was felt that nothing would be achieved by attempting to drill the holes to the planned 1m depth. All holes were back-filled on completion of the sampling.

4.3 The UAV Flights

4.3.1 UAV Flight Procedure

Five flight paths were flown from the seven originally selected. These flight paths are shown in Figure 27. There are sections of the irrigation channel system that were not flown due to time constraints. These are the Flight Path #2 and Flight Path # 3 together with the section of irrigation channel B2 that continues after the western end of Flight Path #5. All of the sections that were not flown during this project were checked during the Risk Assessment stage and visual inspections showed there was not any location that had the potential to be an irrigation channel leak site. Lack of lush vegetation was the prime factor in eliminating these locations. Channel B2 extension from Flight Path #5 was not flown as there had not been water in this irrigation channel.

This rejection of locations was subsequently confirmed to be a correct assessment by the management of Mallowa Irrigation Limited. All flights were flown successfully with no wind interference.

Figure 27

Flight paths flown by UAV during Phase 1.



Note: Source - Base map Bing and (SAS Planet Development Team, 2021) and (Blue Marble Geographics, 2020).

All heights were flown at 80m above ground level. This height was consistent over the whole project as the longitudinal slope of the irrigation channels was minimal. The duration of each flight was less than 20 minutes. The time for each flight depended on the geographical features

of the particular flight path. The UAV height of 80m gave a GSD of 3.9 cm/pixel and produced excellent images. This information was recovered from the metadata attached to the downloaded images. DJI's specifications for the camera used showed that the GSD for this camera can be calculated by the formula

$$\text{GSD} = H/18.9 \text{ (cm/pixel)} \quad (6)$$

where H is the height above ground level (DJI, 2021). This formula produced a GSD of 4.23 cm/pixel so the height maintained by the UAV may have been less than 80m. Mission heights of the UAV are governed by a sensitive barometer built into the aircraft and will have an error factor that has to be considered when planning any flights.

Each image was produced with an 80% overlap in the forward direction and 25% in the lateral direction. Approximately 1064 images were produced for each flight path.

4.4 Suitability of the DJI P4 UAV for This Project and Flight Times

4.4.1 Suitability

The DJI P4 4 UAV, with a multi-spectral camera proved to be ideal for this project. It navigated the planned flight paths correctly, the photo images downloaded from the UAV were perfect for the ortho-photo-mosaic production and there were not any maintenance problems during the flights undertaken. The UAV's flight was stable during this project. Battery life met the expected 20 minutes.

4.4.2 Flight Time

The total flight time for the 19km of irrigation channel under review was two hours. The time taken to move from each flight path's central position to the next flight path's start point is not

included in this time. Time spent waiting for the aerial crop spraying to be finished near Flight Path #4 was not included in this summary.

4.5 Processing of UAV Images

4.5.1 Production of Ortho-Photo-Mosaic Images

Agisoft® Metashape V1.7.4 (Agisoft LLC, 2021) software was used to convert the individual images from the UAV into an ortho-photo-mosaic. An example of an ortho-photo-mosaic is shown as Figure 28.

Figure 28

Ortho-photo mosaic of flight path #6



Note: Source - Agisoft Metashape (Agisoft LLC, 2022).

4.6 Production of the GNDVI Overlay and Masks

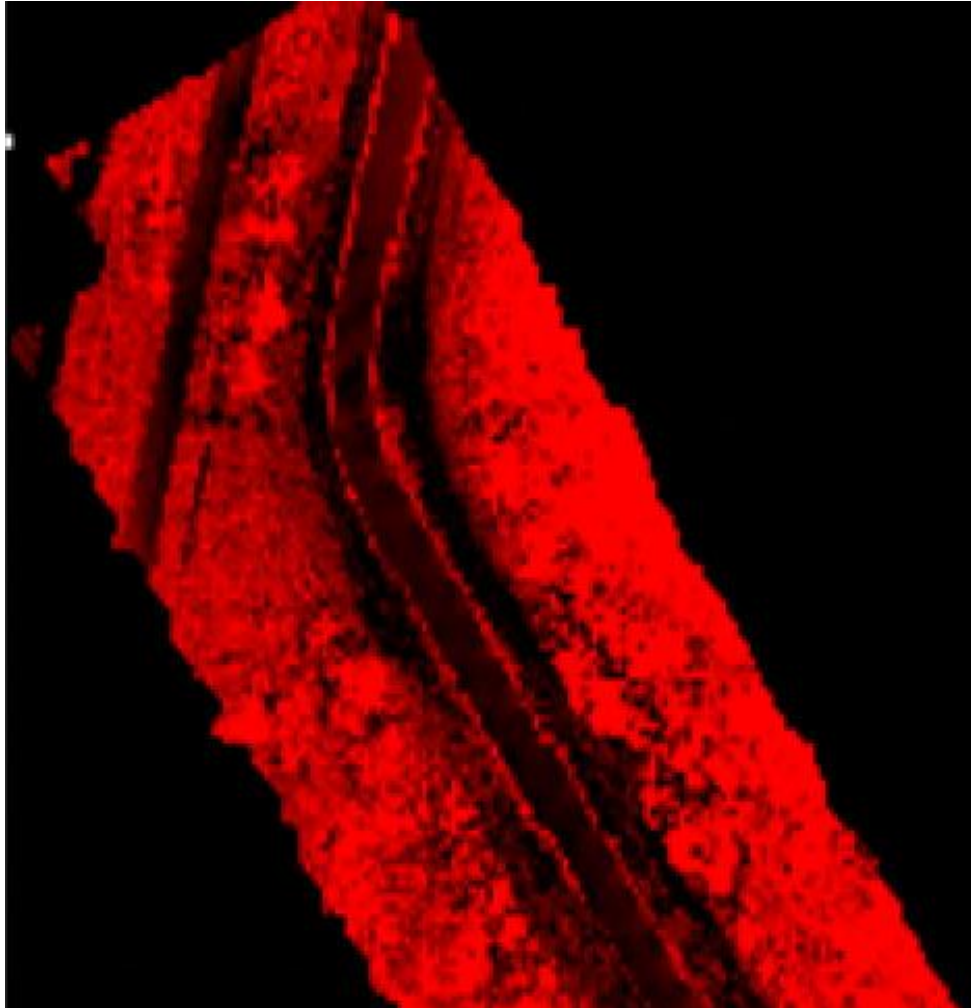
The ortho-photographic-mosaic images were transferred to a desktop PC with 32mb of Random-Access Memory (RAM) for faster processing into GNDVI images using the European Space Agency's SNAP toolkit.

Using the ortho-photo-mosaic image, the eventual aim is to identify the individual pixels with high GNDVI values.

After the ortho-photo-mosaic is installed in the software's Product Explorer the menu choice of Optical Tools – Thematic Land Processing – Vegetation Radiometric Indices – GNDVI is selected. This will create a new file, with GNDVI included in the filename. In this process the algorithm in the ESA SNAP toolbox calculates the GNDVI value for each pixel using the equation (1) on page eight. Each pixel with a GNDVI value greater than -1 is coloured red, without gradient; simply to identify that the pixel has a GNDVI value. Components of the image that are free of vegetation that does not have a GNDVI value are shown as black coloured pixels. This is shown in Figure 29 below. The determination of the GNDVI value for each pixel occurs in the Mask Management process.

Figure 29

GNDVI overlay of ortho-photo-mosaic for Flight Path # 4



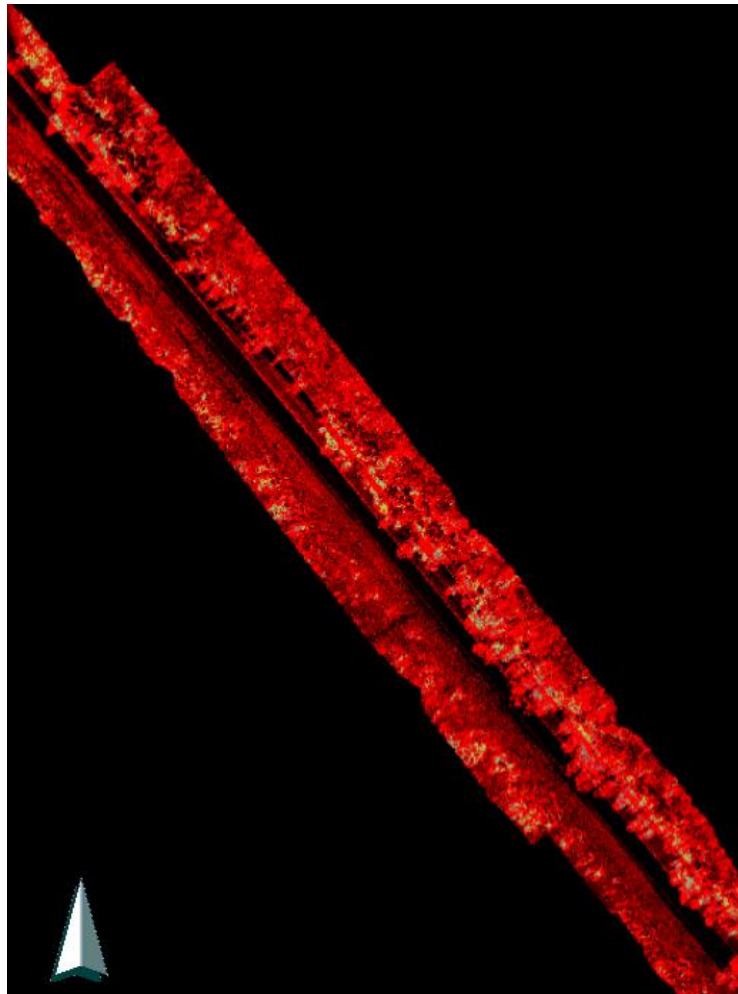
Note: European Space Agency SNAP Toolkit (European Space Agency, 2021).

After the GNDVI overlay is generated the Mask Manager component of the software can now be opened. The Mask Manager allows for the determination of pixels with a high GNDVI value, using values from -1 to +1. In this project the value range set for the mask was for a GNDVI value between a minimum of 0.6 and a maximum of 0.85. Mask values are determined by adjusting the values until hotspots are clearly identified. For Flight path #4 the ideal value to identify the hotspots

was 0.80. Two masks were needed, a yellow and a light blue one to accentuate the irrigation channel hotspot colour. This is shown in Figure 30 below. Table 5 identifies the mask values used.

Figure 30

GNDVI overlay with arithmetic mask overlays



Note: Source-European Space Agency SNAP Toolkit (European Space Agency, 2021).

This process went quickly and flawlessly using the tools provided in the SNAP Toolkit.

Table 4

Mask values used to define hotspots

Flight Path	1	2	3	4	5	6	Remarks
Mask value (Min value)	0.65	0	0	0.80	0.60	0.45	See below for comments on variations
Hotspots found	4	0	0	3	4	2	Vehicle ruts (2) not included in count.

The variation in mask values is caused by the different soil classifications affecting the SMC values on each flight path. This is shown in Table 5 above. Flights #2 and #3 were not flown.

4.7 Plotting the Hotspots on a Map

Co-ordinate locations from potential irrigation channel leak sites were entered into DNRGPS software (Minnesota Department of Natural Resources, 2021). This is a database type of application that saves the information in .gpx format. This data can be added to the commercial software Global Mapper® (Blue Marble Geographics, 2020) to create a visual, georeferenced display of the potential irrigation channel leak sites as shown in Figures 31 and 32 below. The result obtained by interpretation of the hotspot locations for each Flight Path have been plotted on the satellite image map of the irrigation channel systems in the St George area using Global Mapper V24 (Blue Marble Geographics, 2020). These are shown as Figures 31 and 32 below.

Figure 31

Channel B2 top section - hotspots and Soil Moisture Content values



Note: Source – BING Maps and Global Mapper, 2021 (ESRI Aust Pty Limited, 2021 and Blue Marble Geographics, 2020). Global Mapper © Blue Marble Geographics 2020.

Figure 32

Channel B2 bottom section hotspots and Soil Moisture Content



Note: Source – BING Maps and Global Mapper, 2021 (ESRI Aust Pty Limited, 2021 and Blue Marble Geographics, 2020). Global Mapper © Blue Marble Geographics 2020.

There were 12 hotspots identified. In addition, two wheel ruts were identified which were probably created when a vehicle drove over an area with a high SMC at one time; possibly during earlier periods of high rainfall as there was no evidence of high SMC values found at these locations. The second wheel rut location did not show a high SMC value so it may be that during wetter seasons, water from the large nearby dam or the lateral roadside drainage channel along the Castlereagh Highway may be the source of water for this wet spot. The high moisture contents in Figure 31, the top section, identified as BDA1-1 and BDA1-2 may be caused by these points being in the vicinity of the large dam across the road.

A further water problem was found at point BDA6_1 where water is lying in the immediate vicinity of the irrigation channel bank. There was no large vegetation growth on the elevated bank of this irrigation channel so it is felt that this water is coming from the large turkey nest dam to the immediate south of this location.

4.8 SMC from Ground-truthing, USC Classes and Munsell Colours

The SMC values are shown below in Table 6. The highest reading was only 2.97% at location BDA5_2. At this location the grass was noticeably greener than the surrounding grasses. The mean value of SMC for all fourteen holes was 1.41% indicating that channel leakage along this irrigation channel is not a problem. The Munsell Colors (sp) are the soil colour determination from the Munsell Charts based on Hue, Saturation and Chroma. The colours comply with the requirements of Standard Z138.2 of the American Standards National Institute (“Munsell Color Notation & Color Test; Dimensions of Color,” 2011).

Table 5

Soil moisture content from ground truthing.

LOCATION	Lat	Lon	SMC(%)	USC Class	Munsell Colour
Control_1	-28.09614	148.71277	1.01	SC	GLE Y 7 5G
Control_2	-28.14941	148.71813	0.89	SW	10R 8 2
Wheel Ruts #1	-28.08635	148.71218	2.03	OH	GLE Y 7 5G
BDA1-1.1	-28.08673	148.71232	1.95	CL	GLE Y 7 5G
BDA1_1.2			2.28	CL	GLE Y 7 5G
BDA1_1.3			2.39	CL	GLE Y 7 5G
BDA1_2.1	-28.08678	148.71235	1.97	CL	GLE Y 7 5G
BDA1_2.2			2.58	CL	GLE Y 7 5G
BDA1_2.3			2.04	CL	GLE Y 7 5G
BDA1_7.1	-28.09113	148.71381	1.78	CL	GLE Y 7 5G
BDA1_7.2			1.25	CL	GLE Y 7 5G
BDA1_7.3			0.77	CL	GLE Y 7 5G
BDA1_8.1	-28.09118	148.71381	1.16	CL	GLE Y 7 5G
BDA1_8.2			1.63	CL	GLE Y 7 5G
BDA1_8.3			1.54	CL	GLE Y 7 5G
BDA1_9.1	-28.09369	148.71459	1.13	CL	GLE Y 7 5G
BDA1_9.2			0.92	CL	GLE Y 7 5G
BDA1_9.3			1.76	CL	GLE Y 7 5G
BDA4_1.1	-28.161915	148.72212	1.45	SW	5YR 8 2
BDA4_1.2			0.45	SW	5YR 8 3
BDA4_1.3			1.19	SW	5YR 8 4
BDA4_2.1	-28.1615	148.71136	0.52	SW	5YR 8 5
BDA4_2.2			0.39	SW	5YR 8 6
BDA4_2.3			1.15	SW	5YR 8 7
BDA4_3.1	-28.16655	148.72632	1.97	SW	5YR 8 8
BDA4_3.2			0.05	SW	5YR 8 9
BDA4_3.3			0.66	SW	5YR 8 10
BDA5_1.1	-28.16832	148.72705	2.32	SW	5YR 8 11
BDA5_1.2			0.60	SW	5YR 8 12
BDA5_1.3			2.16	SW	5YR 8 13
BDA5_2.1	-28.17165	148.72493	2.97	CL	GLE Y 7 5G
BDA5_2.2			1.55	CL	GLE Y 7 5G
BDA5_2.3			1.44	CL	GLE Y 7 5G
BDA5_3.1	-28.17381	148.72358	0.79	CL	GLE Y 7 5G
BDA5_3.2			1.67	CL	GLE Y 7 5G
BDA5_3.3			1.85	CL	GLE Y 7 5G
Wheel ruts #2	-28.17521	148.72277	1.90	CL	GLE Y 7 5G
BDA5_4.0	-28.17466	148.72273	1.92	CL	GLE Y 7 5G
BDA6_1.0	-28.17507	148.72174		CL	GLE Y 7 5G
BDA6_2.1	-28.18023	148.71324	1.41	CL	GLE Y 7 5G
BDA6_2.2			1.31	CL	GLE Y 7 5G
BDA6_2.3			1.31	CL	GLE Y 7 5G
		Mean	1.41		

Note: The figure highlighted in light blue is the maximum SMC detected.

4.9 Soil Classification Results.

The soil classification results are shown in Table 6. The majority of soil types were classified as CL, inorganic clays of medium to high plasticity, but the samples along Flight Path #4 were SW, gravelly sands as determined under the Unified Soil Classification system (ASC Scientific, 2023). The gravelly sands along Flight Path #4 may have allowed more than normal seepage hence the higher Chl-a values recorded in the GNDVI mask overlay but not supported by the SMC values at that location.

4.10 Control Points

Two control point soil samples were taken in locations away from the influence of irrigation channels or crop irrigation. Only two control points were used as, during the Risk Assessment operation there was no indication major leaks were occurring and that there was little variation in the soil types along the irrigation channel. The first control point was on a vehicle track on the south side of McIntyre farm with a SMC value of 1.01%. The second was on Knights Road, west of the irrigation channel B2. Here the SMC was only 0.89%. These control points' SMC values allowed a comparison with the SMC from the ground-truthing holes.

4.11 Results St George – Phase 2 – April 2022.

4.11.1 Factors Affecting Possible Outcome

The same factors that apply to Phase 1 apply to Phase 2; namely rainfall, grass slashing, ground truthing hole depth and sub-surface flows of water from adjacent dams. These are discussed below.

4.11.1.1 Rainfall.

Rainfall recorded between May 2021 and 12 April 2022 was 466.4 mm compared to the mean annual average of 474.2mm for the years 1997-2022 at St George Airport (Australian Bureau of Meteorology, 2023). This extreme amount of rainfall has led to high SMC levels for all of the surrounding country-side. The consequent grass growth has been greater than in 2021 and may have a detrimental effect on the results obtained.

4.11.1.2 Grass Slashing.

Grass slashing was in process along Flight Paths # 5, 6, 7 and 8. This did not interfere with the flight operations for this project as flights had been performed prior to the tractor and slasher reaching the potential leakage sites. The grass cutting did help, by allowing easier access, in the subsequent ground-truthing and identification of potential leakage sites on the following days.

4.11.1.3 Ground-truthing Holes Depths.

The SMC samples were taken at 300 mm depth instead of 1 m. The same reasons applied as for Phase 1 in April 2021. All holes were backfilled on completion of sampling.

4.11.1.4 Sub Surface Water Flows from Adjacent Dams.

There are large surface dams (Turkey-nest) next to Flight Paths #1, #6, #7 and #8. The high recent rainfall may have created the potential for these dams to overflow. This would create high SMC values between the dam and the banks of irrigation channel. At Flight Path 6, a 1m control hole was dug at position B6-2 and the SMC value at this test hole was 14.68% at 1m depth compared with the SMC of 16.15% at the 300m depth of the nearest hole BDA 6-2, 2.

There was only one A Horizon at location B6-2 with a USC of SC and Munsell Chart Colour of 5YR 5/3. The reason for the high SMC reading is that a nearby Turkey-nest dam had recently overflowed and contributed to the high SMC in surrounding areas. This is confirmed by the SMC value of 14.68% in the test hole dug near hole B6-2. No zero moisture samples were experienced due to the recent heavy rains.

4.11.1.5 Irrigation Channels Planned to be Flown but Not Included.

Flight Paths # 2 and 3 were not flown during this project for the following reasons:

1. Visual inspection plus interpretation of satellite images determined that grass growth along these irrigation channel banks was minimal,
2. The irrigation channels at the locations were partially below ground level compared to above ground level for most of this irrigation system. This may have an impact on measuring visible potential irrigation channel leaks and,
3. Aerial crop spraying was being conducted close to these irrigation channel flight paths and CASA rules do not permit UAV flying in the vicinity of low flying aircraft.

The Flight Path on the irrigation channel alongside of Touhey's Road was not flown as, similar to Phase 1 there was no visible evidence of potential leakage sites. This was confirmed during the Risk Assessment inspection of this section. The Flight Path from the end of Flight Path 8 to the end of irrigation channel B2 was not flown also for the same reason.

4.12 Risk Assessment for Phase 2 Flights and WH&S Induction

In Phase 2 only the irrigation channels along Bundoran Road (B2) and Touhey's Road were inspected for any risk assessment factors. Tree heights were not measured using the Ackuman DKW800 laser ranger and height measurer as the trees along irrigation channel B2 had been measured during Phase 1. Power lines were no higher than 20 m and flights were to be conducted at 80m height.

The WH&S induction, in accordance with Mallowa Irrigation Limited's safety policies was conducted for the flight operator from the University's CASA licenced contractor.

4.13 The UAV Flights

4.13.1 UAV Flight Procedure

During Phase 2 five flight paths were chosen so that, in compliance with CASA's safety rules the UAV remains within Visual Line of Sight (VLOS). Depending on curves in the channel and tree heights the maximum VLOS achievable was one kilometer. By having the UAV take off in the middle of the Flight Path it was possible to cover the maximum length of two km and do so legally. Flight Path #1 was the longest with a total length of 2282 m. To comply with CASA safety rules, it was necessary to chase the UAV in a vehicle to ensure that it remained in VLOS at all times. This flight path was along a straight bitumen road and the UAV was followed by the operator while the vehicle was driven at 15 kph to pace the UAV.

There was no wind during any of the UAV flights and the air temperature was 28 degrees C so haze and mirage were not a problem. However, tree shadows were visible on the downloaded images of Flight Paths # 5 and 6. These images were unsuitable for use in creating an ortho-photo-mosaic of these flight paths and it was necessary for these flights to be flown on the

following day at a later time so that the sun was overhead. This confirms the advantage of being able to scan the downloaded images from the UAV's memory. In this case the scan showed that shade from the trees was a problem and that the flight had to be re-scheduled.

The parameters used for all flights in Phase 2 are shown below in Table 7.

Table 6

Flight Parameters used for Phase 2 Flights

Speed	Height	GSD	Forward overlap	Lateral overlap
3.8m/sec	55m	2.9cm/pixel	80%	25%

The GSD used in Phase 2 was smaller than that used in Phase 1. The original GSD was 3.9cm/pixel. Altering this parameter, combined with a UAV height reduction from 80m to 55m increased the number of .TIFF files to be downloaded from the UAV as the DJI GS Pro software alters the camera shutter timing so that each .TIFF is 4080 kb or .jpg file is between 900 and 1000kb. In Phase 1 for a similar Flight Path 1 there was 1751 .TIFF files. In Phase 2 this number increased to 2514 for the reasons stated above.

4.14 Suitability of the University's NEW DJI P4 UAV

This new UAV was trouble free on its first working flights. Because the GSD was lower and the flight height lower, higher resolution and better quality images were obtained than in Phase 1. Only three batteries came with the original equipment but these three were supplemented with batteries from the flight contractor.

4.15 Flight Times, the Use of Real Time Kinetics System and Flight Patterns

The flight distance for Phase 2 flights was 8485m. Three and a half hours were used in Phase 2, compared to two hours for Phase 1. The University's DJI P4 UAV is fitted with a Real Time Kinetics System (RTK) which utilises a TimeSynch® system to provide 1cm horizontal and 1.5cm vertical accuracy to the geo-referenced images taken by this UAV. The TimeSynch signal comes from either the GPS, Glonass, Galileo or BeiDou satellite systems or a combination of any of these satellites, depending on the location (Enterprise, 2022). Up to 15 minutes was spent at take-off locations getting a strong enough RTK signal to start the flight mission.

A further increase in flight times was caused by the UAV flying a Zig-Zag pattern (determined by the software) to fully cover both sides of the irrigation channel. On the return flight the UAV flew the alternate to the original Zig-Zag pattern. Using this Zig-Zag pattern guaranteed that there was 100% coverage of the irrigation channel banks on both sides together with the lateral access roads. The flight times did not include time spent moving between locations or spent observing agricultural aircraft flying near Flight Paths # 2 and 3.

4.16 Processing of UAV Images.

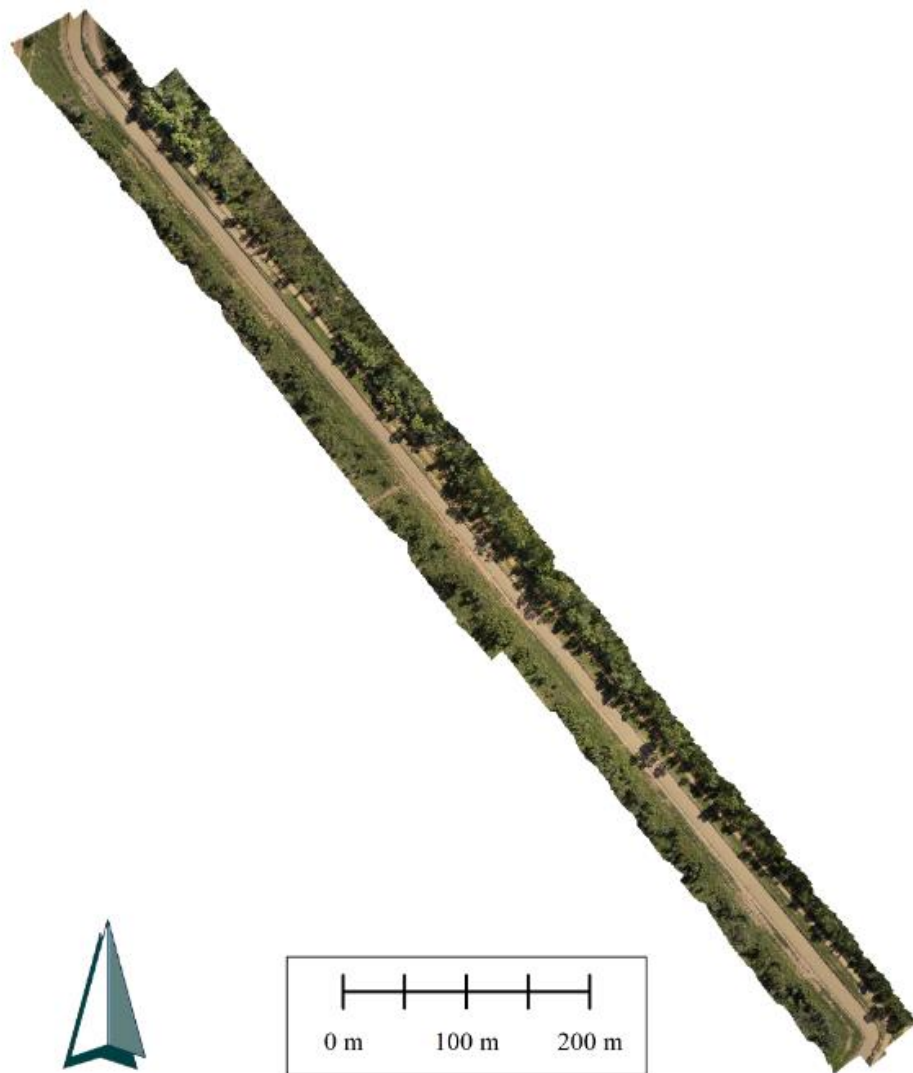
4.16.1 Production of the Ortho-Photo-Mosaic Images

In this second Phase Agisoft ® Metashape Pro V1.82 (Agisoft LLC, 2021) was used to convert the individual images downloaded from the UAV into an ortho-photo-mosaic image. The same process steps as detailed in Phase 1 was used and an example of the finished product is shown

at Figures 33 and 34 below. Figure 33 is the Ortho-photo-mosaic of Flight Path #5, built from .jpg files.

Figure 33

Ortho-photo-mosaic of Flight Path # 5



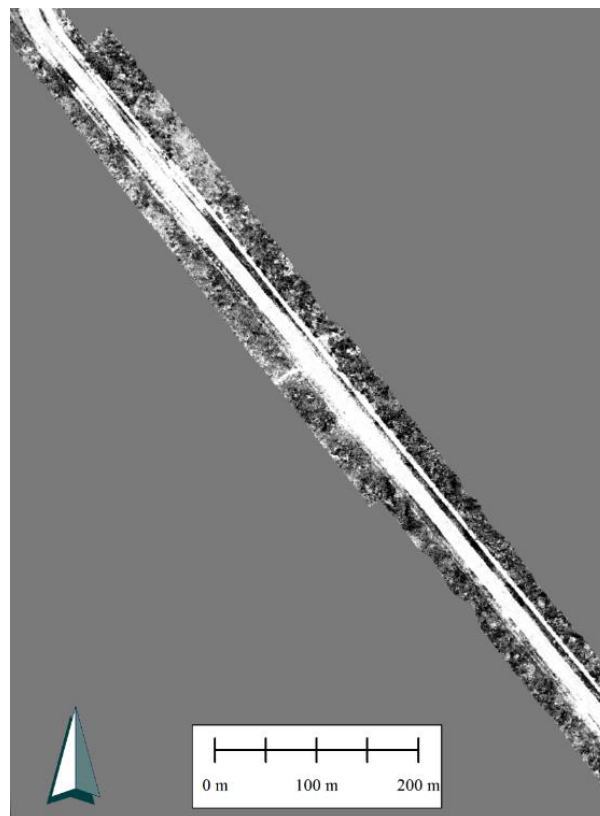
Note: Source: DJI P4 UAV and Agisoft ® Metashape V1.82 (Agisoft LLC, 2022).

4.16.2 Production of GNDVI Overlay

The production of the GNDVI overlay was achieved using the European Space Agency SNAP Toolboxes (European Space Agency, 2021). The process has been fully described in Phase 1 of these results. A section of the GNDVI overlay for Flight Path #5 is shown below as Figure 34. The new version (1.8.2) of Agisoft Metashape ® produces a different colour image than Version 1.7.2 used in Phase 1.

Figure 34

GNDVI Map of Flight Path # 5



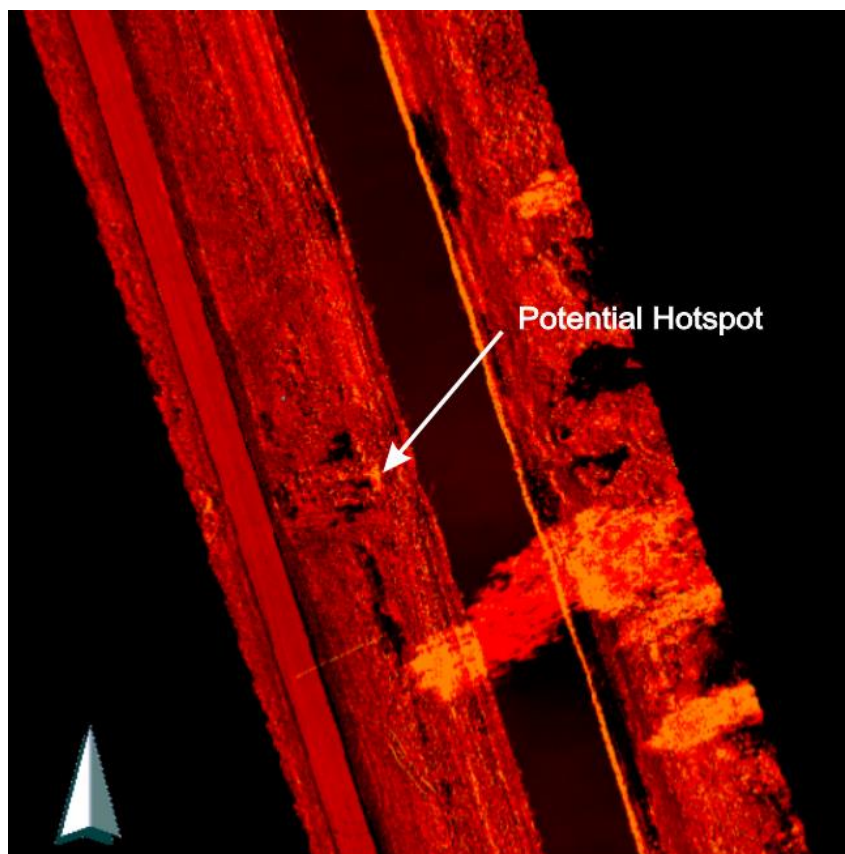
Note: Source: DJI P4 UAV and Agisoft ® Metashape V1.82 (Agisoft LLC, 2022). This is the second flight along Flight Path #5; re-flown to eliminate tree shadows.

4.16.3 Calculating GNDVI Values Using the Mask System in the European Space Agency's SNAP Toolbox

When the GNDVI overlay is complete the software in the ESA SNAP toolbox allows a mask to be created. This mask, depending on the values set, will stop the colouring of pixels in the GNDVI overlay at the maximum value which is determined when the leakage hotspots are revealed. An example of this is shown in Figure 35 below where the mask value was set between 0.58 and 0.8. GNDVI detected pixels outside of this range do not appear.

Figure 35

GNDVI overlay with arithmetic mask value of between 0.58 and 0.8



Note: Source – European Space Agency SNAP Toolbox (European Space Agency, 2021).

4.16.4 Plotting the Results on a Map

Similar to this same function in Phase 1 the results were plotted on the quality ortho-photo-mosaic (red, green, blue bands) produced from the DJI P4 UAV images using Agisoft Metashape ®. Co-ordinate locations from potential irrigation channel leak sites were entered into DNRGPS software (Minnesota Department of Natural Resources, 2021). This is a database type of application that saves the information in .gpx format. This data can be added to the commercial software Global Mapper® (Blue Marble Geographics, 2020) to create a visual, georeferenced display of the potential irrigation channel leak sites as shown in Figures 36 to 41.

Figure 36

Identified hotspot at Flight Path #1



Note: Source: DJI P4 UAV ortho-photo-mosaic plus Global Mapper (Blue Marble Geographics, 2020) and European Space Agency SNAP Toolbox Application (European Space Agency, 2021.)

Figure 37

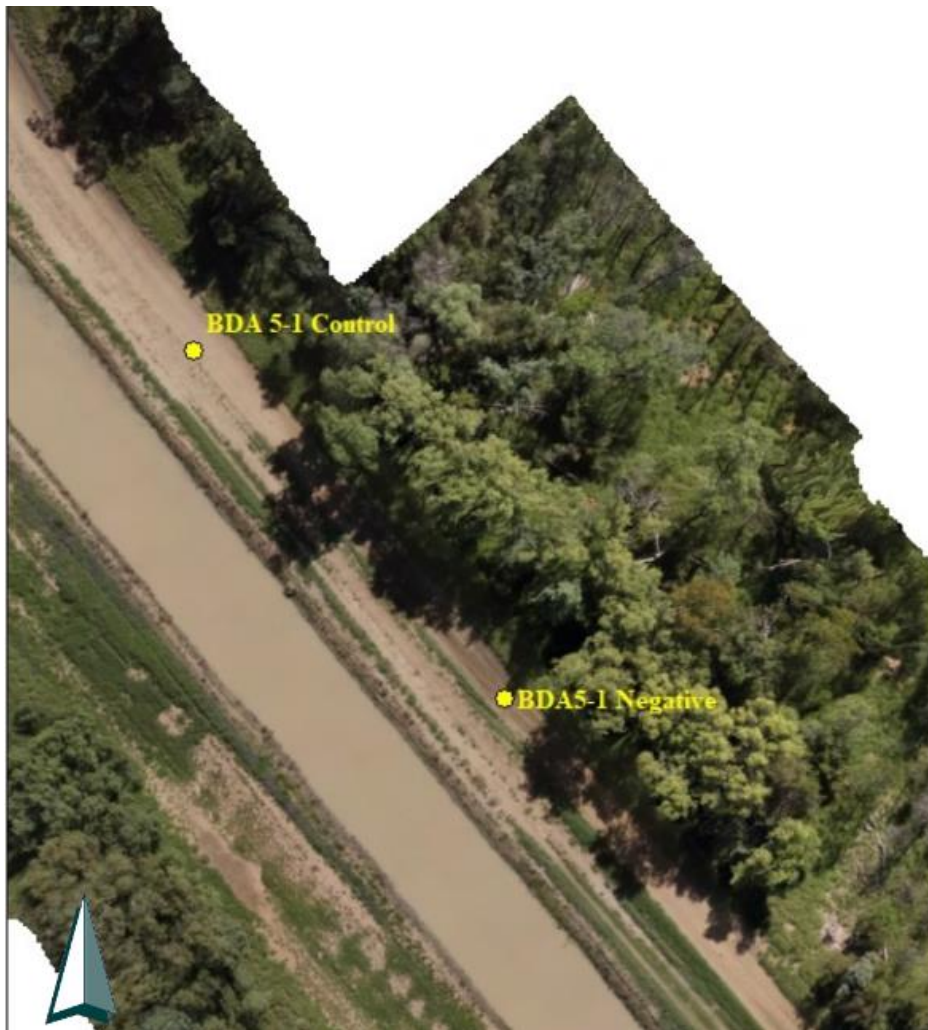
Identified hotspot at Flight Path # 4



Note: Source: DJI P4 UAV ortho-photo-mosaic plus Global Mapper (Blue Marble Geographics, 2020) and European Space Agency SNAP Toolbox Application (European Space Agency, 2021).

Figure 38

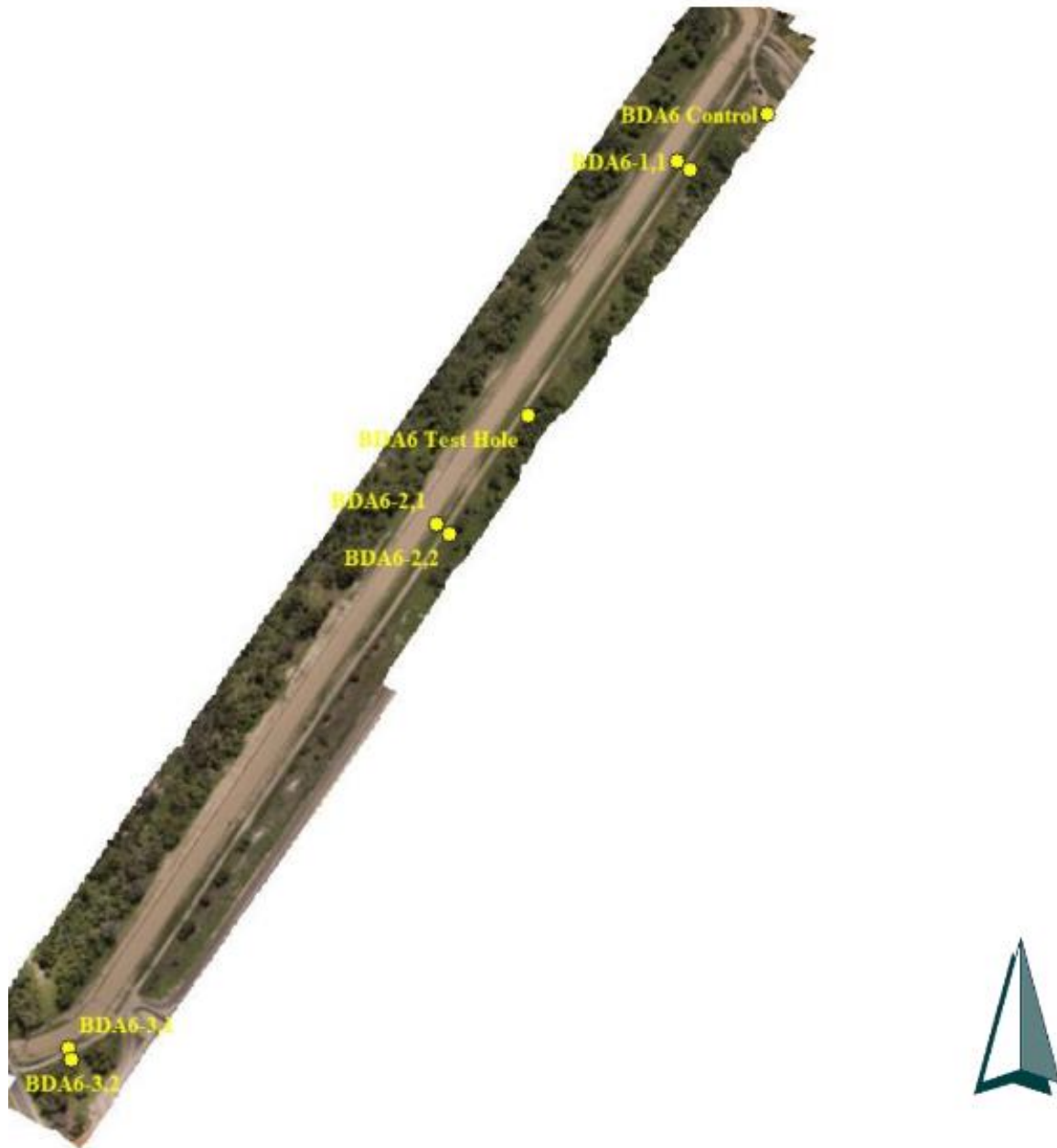
Identified hotspot at Flight Path # 5



Note: Source: DJI P4 UAV ortho-photo-mosaic plus Global Mapper (Blue Marble Geographics, 2020) and European Space Agency SNAP Toolbox Application (European Space Agency, 2021).

Figure 39

Identified hotspots at Flight Path # 6



Note: Source: DJI P4 UAV ortho-photo-mosaic plus Global Mapper (Blue Marble Geographics, 2020) and European Space Agency SNAP Toolbox Application (European Space Agency, 2021)

Figure 40

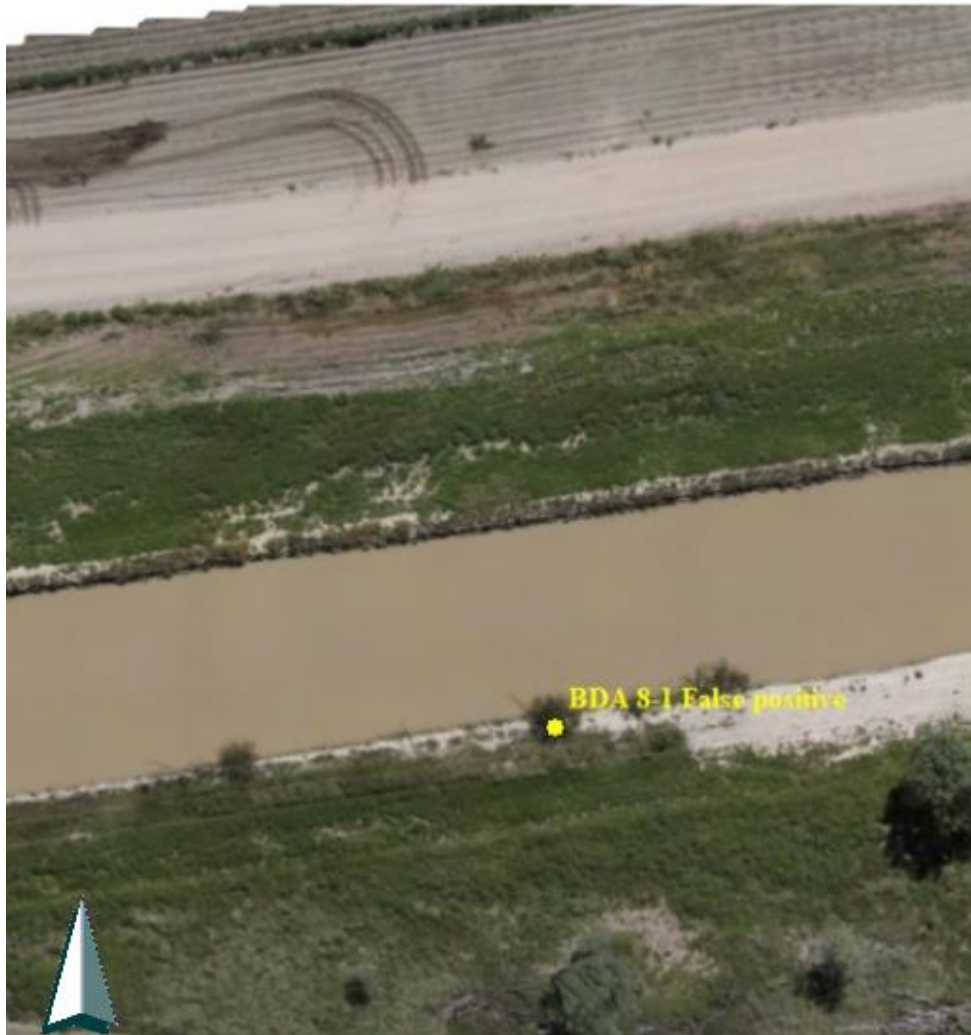
Identified hotspots at Flight Path #7



Note: Source: DJI P4 UAV ortho-photo-mosaic plus Global Mapper (Blue Marble Geographics, 2020) and European Space Agency SNAP Toolbox Application (European Space Agency, 2021).

Figure 41

Identified hotspots at Flight Path #8



Note: Source: DJI P4 UAV ortho-photo-mosaic plus Global Mapper (Blue Marble Geographics, 2020) and European Space Agency SNAP Toolbox Application (European Space Agency, 2021).

4.16.5 Potential Leak Site Identifications

The potential leak sites identified from the UAV images totalled seven and are shown in Table 9 below. During the ground truthing stage a further potential leak site was discovered along Flight Path #5, as a false negative by visual inspection and confirmed by collection of SMC

samples. A further false positive from the interpretation of the ortho-photo-mosaic was located on Flight Path #8. This was subsequently confirmed to be a high Chl-a Common Pear Cactus (NSW Dept of Primary Industry, 2022).

The potential leak sites along Flight Path #6 and # 7 may be caused by either seepage from adjacent land which is semi-saturated due to the recent heavy rains or leakage from the two large dams on either side of the Carnarvon Highway where Flight Path # 6 ends and Flight Path #7 begins. This is supported by the higher SMC values from the ground truthing holes numbered BDA6-1,2, BDA6-2,2 BDA6-3,2 and BDA7-1,2 taken during this project.

The potential leak site along Flight Path # 5, identified from the false negative is 18.1m SSE of the potential leak site identified in Phase 1. This was measured on the ortho-photo-mosaic using Global Mapper®. A full list of potential irrigation channel leakage sites is shown as Table 8 below.

Table 7*Soil moisture contents, USC Classes and Munsell Colours*

Location	Latitude	Longitude	Wet Weight	Dry Wt	SMC	Soil Type	Munsell Colour
BDA1_1	-28.087870	148.712760	208.93	198.67	5.16	SM (gray)	GLE Y 8/1
BDA1-2	-28.088948	148.712984	123.57	118.60	4.19	SM (gray)	GLE Y 8/1
BDA1 Control	-28.095275	148.714431	208.66	195.57	6.69	SM (gray)	GLE Y 8/1
BDA4-1, 1	-28.151790	148.722730	206.51	190.82	8.22	SC(gray)	
BDA4-1,2	-28.151742	148.722784	178.33	171.30	4.10	SC(gray)	7.5 YR 5/ 2
BDA4 Control	-28.151832	148.722822	167.23	159.49	4.85	SM (light gray)	7.5 YR 3/ 2
BDA 5-1 Negative	-28.161281	148.722026	203.68	189.91	7.25	S	5YR 6/ 3
BDA5-1,2	-28.161233	148.722075	268.64	252.39	6.44	S	5YR 6/ 3
BDA 5-1 Control	-28.160978	148.721755	167.23	159.80	4.65	S	5YR 4/ 3
BDA6-1, 1	-28.168767	148.726712	153.89	139.25	10.51	SM (light gray)	5YR 5/ 6
BDA6-1,2	-28.168742	148.726849	133.51	115.32	15.77	SM (light gray)	5YR 5/ 3
BDA6-2, 1	-28.171201	148.725105	227.58	204.36	11.36	SM (light gray)	5YR 5/ 6
BDA6-2, 2	-28.171246	148.725186	179.37	154.43	16.15	SM (light gray)	5YR 5/ 3
BDA6-2 Test hole	-28.170729	148.725503	371.46	323.91	14.68	SM (light gray)	5YR 5/ 3
BDA6-3, 1	-28.174740	148.722518	214.82	188.76	13.81	SM (light gray)	10YR 4/ 6
BDA6-3, 2	-28.174804	148.722629	169.00	149.03	13.40	SM (light gray)	5YR 4/ 4
BDA6 Control	-28.168562	148.727352	181.29	163.67	10.77	SM (light gray)	5YR 5/ 6
BDA7-1, 1	-28.179770	148.715614	187.64	173.90	7.90	MC (gray)	7.5YR 5/ 3
BDA7-1, 2	-28.179852	148.715544	234.48	215.90	8.61	MC (gray)	7.5YR 5/ 3
BDA7 Control	-28.179525	148.715330	149.88	141.04	6.27	MC (gray)	7.5YR 5/ 3
BDA8-1, 1	-28.181425	148.700609	NIL				

4.16.6 Variation in Munsell Colours from Phase 1

A different book of colour charts was used for Phase 2 proving a more accurate interpretation. The soil samples were oven dried at 110⁰C for a period of six days (over a holiday period) and this may have partially contributed to the colour differences. This six-day period is much greater than the 16 hours recommended in Australian Standard AS1289 B1-1 (NSW Department of Sustainable Natural Resources, 1990). Also, the soil colours were checked against USQ's Munsell colour chart book compared to internet publications used in Phase 1.

4.16.7 Interpretation of Data from Table 8

Table 9 below shows each detected potential hotspot and has the reason for that point's identification.

Table 8

Interpretation of Data

Hole Identification	Remarks
BDA 1-1	Run off from Bundoran Road bitumen surface.
BDA 4-1	Spillage from overfull irrigation channel.
BDA 5-1	Potential leak. Not seen on masked image. False negative. SMC above control value.
BDA 6-1, 6-2 and 6-3	High SMC values but the high test hole value and individual SMC values suggest that water is seeping towards the channel from adjacent large dam.
BDA 7-1	Potential leak but also adjacent to large dam.
BDA8-1	False positive. No SMC value taken as hotspot identified as large cactus during ground truthing.

4.16.8 Influence of Recent Heavy Rainfall

There has been heavy rainfall in this region and from satellite imagery all of the large dams appear to be full and some may have overflowed with this excess water flowing towards the base of the irrigation channel. This could be the contributing factor of the SMC readings in the ground-truthing holes; especially along Flight Path #6. This theory is supported by the SMC value of 14.68% from the 1m test hole dug between holes BDA 6-1 and BDA 6-2.

4.16.9 Soil Classification Results

The soil classification results are taken from Table 9. The majority of the soil types are classed as CL, an inorganic clay of medium to high plasticity but the samples along Flight Path #4 and #5 were SW, gravelly sands as determined by the USC System. This gravelly sand patch may have allowed higher seepage rates than normal along Flight Path #5 leading to the 50m long damp patch on the surface of the adjacent track that produced the false negative reading.

4.17 Use of alternate radiometric vegetation indices

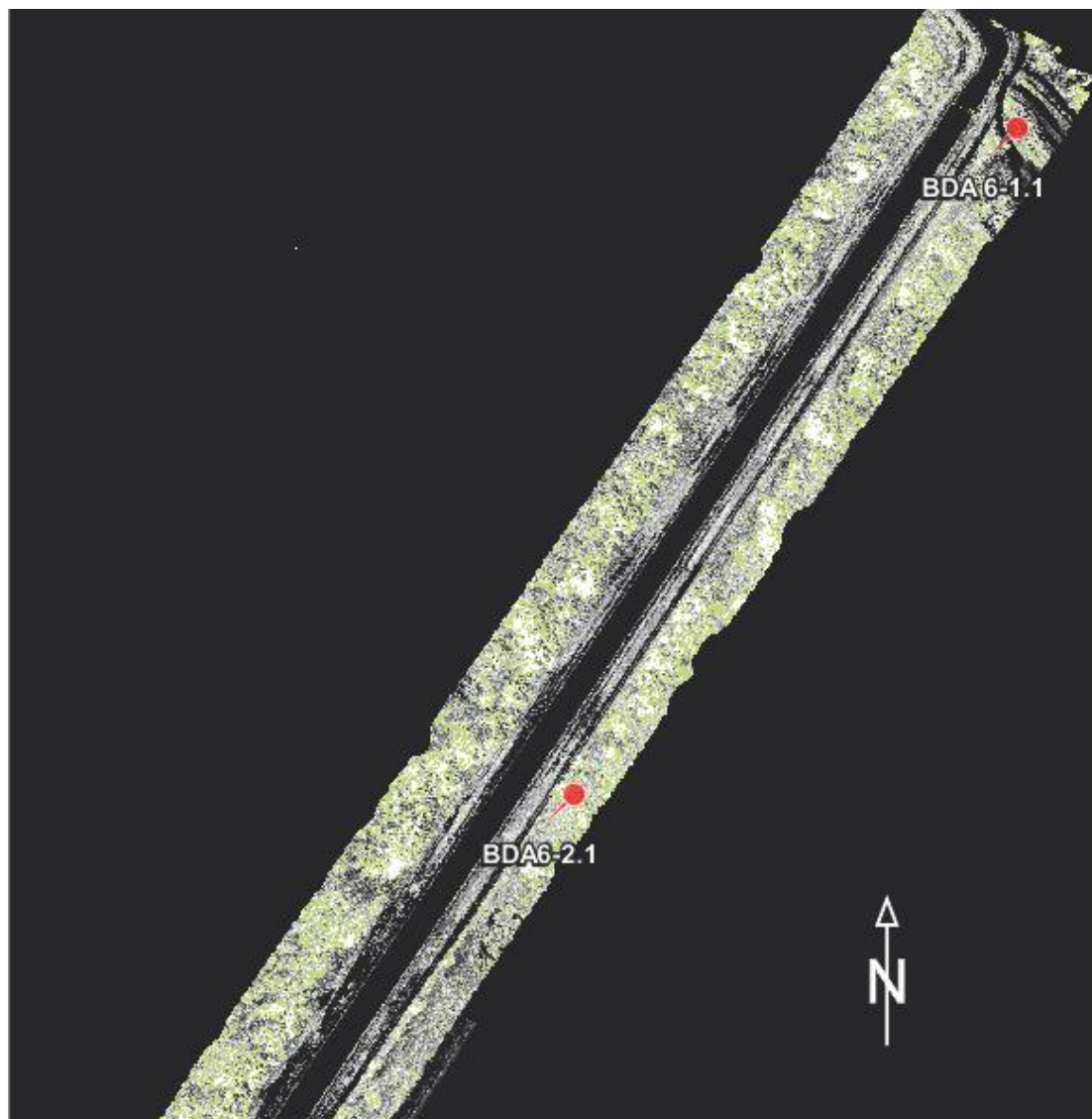
4.17.1 Selection of Appropriate Radiometric Vegetation Indices


A comparison was made with vegetation indices other than GNDVI. The four chosen from Table 1 that have the closest relationship to GNDVI are:

1. The Normalized Difference Vegetation Index (NDVI) using the Red and NIR Bands. NDVI is sensitive to soil brightness, soil colour, atmosphere, cloud shadow and leaf canopy shadow (Earth Observing System, 2017). These are all factors that have a potential to affect the results achieved from using this index. Figure 42 below is part of the ortho-photo-mosaic for Flight Path #6. It can be seen that the NDVI Index has not identified the high Chl-a growth at points B6-1, 1 and B6-2, 1.

Figure 42

NDVI Mask for Flight Path #6



 **Legend**
Hotspot identified by
GNDVI process but not by
NDVI process.
NDVI mask shown in light
green.

Note: Source - DJI P4 UAV ortho-photo-mosaic plus Global Mapper (Blue Marble Geographics, 2020) and European Space Agency SNAP Toolbox Application (European Space Agency, 2021).

2. The Transformed Normalized Difference Vegetation Index (TNDVI) uses the NIR and Red Bands and is used for identifying the strength of vegetation.

The formula for calculating this vegetation index is shown below as equation 10 (Gouri & Manjula, 2019):

$$\text{TNDVI} = \sqrt{\text{NDVI} + 0.5} \quad (10)$$

An example of the TNDVI overlay is shown below as part of Flight Path #6 at Figure 43. Neither of the two potential irrigation channel leak sites is identified.

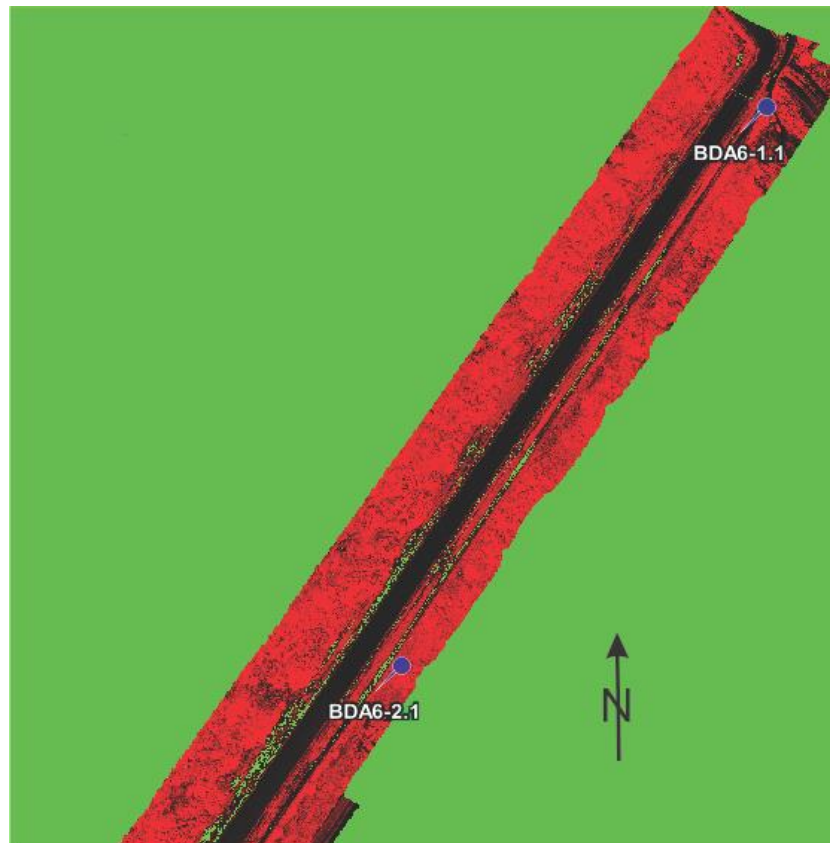
3. Difference Vegetation Index (DVI). This index shows the differences between soil and vegetation (Harris Geospatial Systems, 2018). DVI has the disadvantage of ignoring atmospheric parameters or shadows. Uses the formula:

$$\text{DVI} = \text{NIR} - \text{red} \quad (11)$$

In Figure 45, below, it can be seen that although the mask values were coloured yellow there are no recognisable yellow hotspots on the image. The two known GNDVI hotspots on this image have blue pin markers.

Figure 43

Transformed Normalized Difference Vegetation Index



Legend
● Hotspot identified by GNDVI process but not by TNDVI process.
TNDVI mask shown in green.

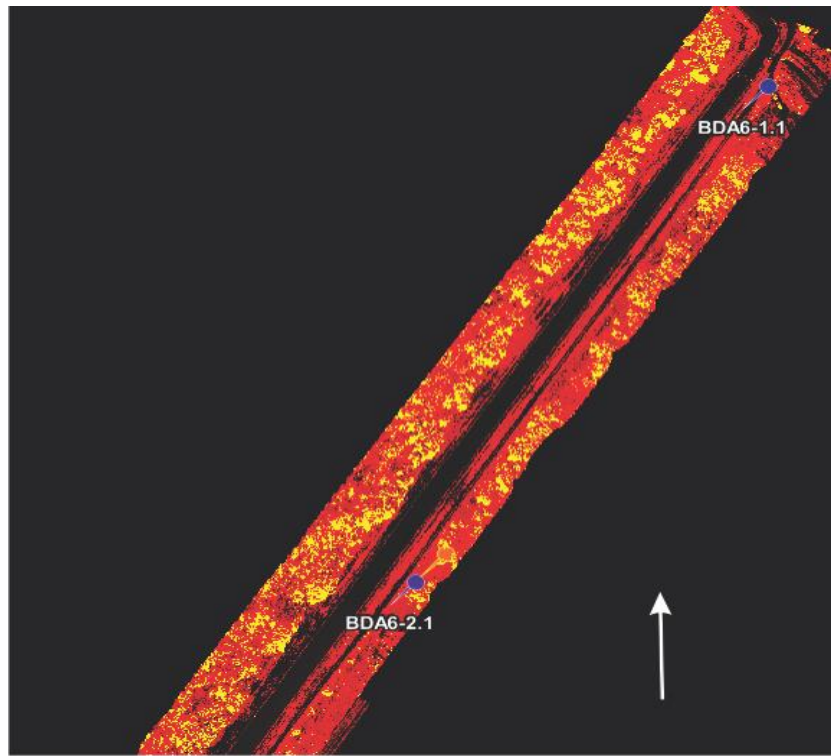
Note: Source - DJI P4 UAV ortho-photo-mosaic plus Global Mapper (Blue Marble Geographics, 2020) and European Space Agency SNAP Toolbox Application (European Space Agency, 2021).

The Soil adjusted vegetation index (SAVI) is used to minimise the influence of soil factors on the vegetation index (Qi et al., 1994). This index has improved sensitivity to soil background. With tall vegetation the soil background has limited effect on the values recorded. Vegetation heights of at least 1m occur along the irrigation channel banks in this project. Part of Flight Path # 6 is shown below as Figure 44. It can be seen that the identified high Chl-a sites

previously identified have not been located but all the vegetation along the irrigation channel banks has been highlighted.

Figure 44

Soil adjusted vegetation index overlay

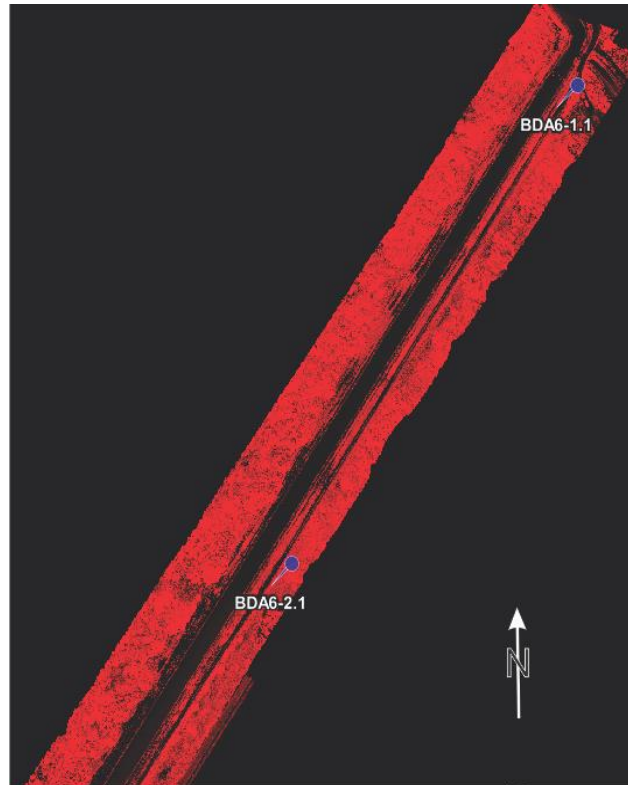


Legend
● Hotspot identified by GNDVI process but not by SAVI process.
SAVI mask shown in yellow.

Note: Source - DJI P4 UAV ortho-photo-mosaic plus Global Mapper (Blue Marble Geographics, 2020) and European Space Agency SNAP Toolbox Application (European Space Agency, 2021).

Figure 45

DVI Vegetation Index



Legend
● Hotspot identified by GNDVI process but not by DVI process.
DVI mask coloured yellow but is not visible.

Note: Source - DJI P4 UAV ortho-photo-mosaic plus Global Mapper (Blue Marble Geographics, 2020) and European Space Agency SNAP Toolbox Application (European Space Agency, 2021).

The four comparisons had the Mask Value of the vegetation indices set at a range between 0.50 and 0.8. The scale of all of the vegetation indices used is from -1 to +1 and is shown in Table 10.

Table 9

Mask values used to define potential leak hotspots

Flight Path	1	2	3	4	5	6	7	8	Remarks
Mask Value (Min value)	0.6	0	0	0.6	0.60	0.58	0.62	0	Flight Path #2 and 3 not flown
Hotspots found	0	0	0	1	1	3	2	1	False positive at Flight 8

4.18 Other Software Applications that Produce Vegetation Indices

4.18.1 Other Applications

There are several software applications that can produce images with vegetation indices calculated for each pixel in an ortho-photo-mosaic. Some of these are ENVI Lidar V 5.3.1 (L3Harris Geospatial Solutions, Inc., 2022), Agisoft ® Photoscan (Agisoft LLC, 2021), SPRING (Camra et al., 1996) and CARTOMORPH (Aguiar et al., 2018).

Each of the above applications are dealt with separately:

1, ENVI Lidar V5.3.1. The toolbox included in this software does not include an algorithm for calculating GNDVI index values in the Radiometric Correction Selection but only NDVI values. The Vegetation Index Calculator requires spectral band wavelengths to be defined so as to calculate vegetation indices. However, this information is not included in the metadata of ortho-photo-mosaic .tiff files available for this project (Excelis Visual Information Systems Inc., 2015). Also, ENVI Lidar V5.3.1 (Harris Corporation, 2015) has the ability to process vegetation indices; requiring two or more spectral bands. However, this application will not process .tiff or .jpg files. The software produces the error message “File does not contain text

fields”. This makes the software unsuitable to use in this project as the collected images from the UAV are either .jpg or .tiff files.

2. AGISOFT® PHOTOSCAN. This application only calculates NDVI values based on multi-spectral imagery (ortho-photo-mosaic) (Position Partners, 2021). The calculated data can be exported as a grid of floating-point index values calculated by pixel from the ortho-photo-mosaic. However, this application has been developed for specific equipment; namely the Parrot Sequoia UAV (Sphere Drones Australia, 2022) and the MicaSense RedEdge® multi-spectral camera (MicaSense Limited, 2018).

3. SPRING. Developed by the Brazil National Institute for Space Research in 2017. It is a GIS and remote sensing application using an object-oriented database model. This database is made up of Geo-fields containing data including details for image segmentation, regional classification information such as soil maps, topographical maps, slope maps and metadata from satellite images. SPRING can utilize both raster and vector data in the same process (Camra et al., 1996). However, much simpler software applications are now available.

4. CARTOMORPH. Developed by the Department of Cartography, Sao Paulo University, Brazil. This software is a public domain software, designed to provide open software for feature extraction from images and operations between bands on remotely sensed images. Again, this software has only been developed to calculate NDVI index values. Of note, in the conclusion in this paper is the statement “No discrepancy occurred in the output between this software, SPRING and ENVI software (Aguiar et al., 2018).

4.18.2 Summary of Other Applications to Produce Vegetation Indices

The four software options reviewed above do not provide the clean, simple method of producing GNDVI outputs that the European Space Agency's SNAP Toolkit does. Therefore, the SNAP toolkit has been used in this project.

4.19 Discussion

4.19.1 Variation in Hotspot Count Between Phase 1 and Phase 2

During Phase 1 (April 2021) 12 hotspots were identified while in Phase 2 only eight hotspots were discovered even though more rain had fallen prior to Phase 2 (April 2022) flights. Vegetation growth may be one contributing factor. In 2021 there had been less rainfall and correspondingly less grass. This probably contributed to less vegetation growth and better detection of higher GNDVI hotspots. In 2022 vegetation growth was more denser having been stimulated by the higher summer rainfall prior to the UAV flights. This widespread, denser vegetation may have masked the higher GNDVI locations and contributed to lesser identification of hotspots.

4.19.2 Discussion About this project

This project has shown that the potential exists for the use of UAVs to detect possible leaks in irrigation channels. Any leak may lead to a disaster for irrigation management or the end-user irrigator. Once the UAV flights had been completed and the ortho-photo-mosaic image created then the main software contributor was the European Space Agency's SNAP toolbox which allowed a rapid and decisive determination of potential leak sites.

Because Phase 2 was flown at the lower height of 55m and the GSD was shown to be 2.9 cm/pixel, higher definition images have been achieved. The ortho-photo-mosaic images in

Phase 2, as shown in Figure 46 below, can be magnified from the opening scale of 1:4204 to a scale of 1:98.5 where individual plants and water weed patches are still visible.

Figure 46

Flight Path #6 Zoomed image to 1:98.5 with visible weed growth and people



Note: Source - DJI P4 UAV image as ortho-photo-mosaic. Agisoft ® Metashape V1.8.2 (Agisoft LLC, 2022) with Global Mapper (Blue Marble Geographics, 2020).

The GSD of 3.9 cm/pixel used in Phase 1 may have caused the irregularity in the number of sites identified as potential leakage sites.

The high-resolution data from the UAV images is beneficial in the intensive monitoring of irrigation channels and leads to determination of potential hotspots for irrigation channel leakage. UAV images are low cost and provide fast mapping of lengths of irrigation channels. They are available immediately after the UAV flight and are not affected by cloud or atmospheric interference, as may occur with expensive satellite images. The purchase of satellite images to cover the small areas involved with irrigation channels would not be a cost-effective operation. The images available from a UAV multi-spectral camera are very high resolution at 2.9 cm/pixel GSD. The use of an UAV is available at any time which may be a critical factor if an irrigator advises that his crop is being water-logged and will allow a rapid determination the cause of this problem and immediate rectification of any potential leak before it becomes a major problem.

4.19.3 Satellite Imagery Comparisons

Satellite imagery does not provide comparable high enough resolution to identify a potential irrigation channel leak; which may only be several meters in diameter. An example of this is the Sentinel 2 satellite Super Resolution image has a resolution of 10m per pixel. So, if the irrigation channel and banks is less than 10m wide satellite imagery would not be helpful in locating any potential leaks. To be effective a satellite image has to be one meter or better per pixel. Harris Geospatial Solutions (Harris Geospatial Solutions Inc, 2021) suggest that a one-meter resolution satellite image may cost \$10 a square kilometer with a minimum purchase of 100 sq km. If satellite images are purchased, they need to contain the red, green, blue and near-infrared bands where-as all this data is immediately available from an ortho-photo-mosaic image from a UAV multi-spectral camera.

5 CHAPTER 5: CONCLUSION

5.1 Functionality of the System.

5.1.1 *Did the System Work?*

The system worked as planned and the aim of this project was achieved. At St George, hotspots were identified but the low SMC values from the ground-truthing holes during Phase 1 and Phase 2 confirmed that major leakage was not occurring in the system along the Bundoran Road irrigation channel. Comparing the SMC values obtained with the control point values it can be determined that the hotspots located on the GNDVI mask overlay are probably the result of natural seepage due to the nature of the soil type in the irrigation channel wall, together with high seepage from adjacent dams. Increases in moisture level due to different soil compositions are visible in the UAV imagery but do not relate to actual irrigation channel leakage. The management of Mallowa Irrigation Limited concurred with the findings during both Phases of this project.

Testing using alternate soil vegetation indices were all unsuccessful, confirming that the choice of the GNDVI for this project is the appropriate one.

5.1.2 *Confirmation of the UAV's Effectiveness*

The UAV was highly effective in collecting the images for determining if leaking was occurring along the irrigation channels. Although the system did not produce evidence of major irrigation channel leakage it did produce positive results that there were no large irrigation channel leakage hotspots at St George. The system did work and produced positive results for potential irrigation channel leak sites.

These results will allow the irrigation managers to maintain inspections of the potential irrigation channel leak sites on a regular basis.

5.1.3 Effects of Soil Type on Potential Irrigation Channel Leaks

Using the data from Tables 6 and 8 it can be seen that the majority of potential leaks in this irrigation system may occur where the soil type is SM, a well graded sandy silt. This material has a high porosity and this leads to the potential for irrigation channel leaks to occur in the region of Flight Path # 6.

The false negative occurrence on Flight Path #5, occurs in a soil type S, well graded sand. This has a high porosity also and may lead to more potential irrigation channel leaks that are detectable by the use of UAV.

All potential leak sites, except the one on Flight Path #5, shown in Figure 42 at location BDA5-2 Negative were detected by the UAV and subsequent software processing. The large cactus on Flight Path #8. Figure 45, gave a false positive reading but was eliminated as a potential leak site during the ground-truthing stage.

The flight sections that did not exhibit any potential sites for leakage were either located in a poorly graded sand with clay (class SC) or a poorly graded sand with silt (class SM).

5.1.4 Future Work

Future work in the field of irrigation channel leak detection will centre on the use of newer and more sophisticated cameras. An example of this is the Hyperspectral UV-VIS-NIR Video Camera ULTRIS X20 (Cubert-GmbH, 2020). This camera has the capability to capture light from the 350 to the 1000 μm wavelength which goes from the ultra-violet to the microwave

bands, with 164 separate bands discernible. The other factor of this camera is that with the appropriate software it can read directly the Chl-a value of vegetation under surveillance. Other future work will look at the UAV itself. Longer battery life, greater than the current 30 minutes and greater stability in winds higher than 10m/sec (Wingtra AG, 2019) will all contribute to better UAV operations.

Also, this research using UAVs for irrigation channel leak detection could be expanded to incorporate the application of machine learning to automatically detect and interpret potential irrigation channel leak sites.

6 REFERENCES

- Agapiou, A., Alexakis, D. D., Themistocleous, K., Sarris, A., Perdikou, S., Clayton, C., & Hadjimitsis, D. G. (2014). Investigation of Ground Remote Sensing Techniques for Supporting an Early Warning Water-Leakage System. In D. G. Hadjimitsis, A. Agapiou, & K. Themistocleous (Eds.), *Integrated Use of Space, Geophysical and Hyperspectral Technologies Intended for Monitoring Water Leakages in Water Supply Networks*. InTech. <https://doi.org/10.5772/59531>
- Agisoft LLC. (2022). *Agisoft Metashape*. <https://www.agisoft.com/>
- Agisoft LLC. (2021). *Agisoft Metashape User Manual* (Professional edition). Agisoft LLC. https://www.agisoft.com/pdf/metashape-pro_1_7_en.pdf
- Aguiar, T. O., de Azevedo, S. C., Pedrosa, M. M., Cardim, G. P., & da Silva, E. A. (2018). Multispectral Image Processing System Developed in CARTOMORPH Software—NDVI Module. *Advances in Remote Sensing*, 07(02), 91–100. <https://doi.org/10.4236/ars.2018.72007>
- Airport Guide. (2022). *St George Airport—YSGE - SGO - Airport Guide*. AirportGuide. <https://airportguide.com/airport/info/SGO>
- Alamirew, T., & Eshetu, B. D. (2018). Estimation of Seepage Loss in Irrigation Canals of Tendaho Sugar Estate, Ethiopia. *Irrigation & Drainage Systems Engineering*, 07(03). <https://doi.org/10.4172/2168-9768.1000220>
- Artiola, J. F., Pepper, I. L., & Brusseau, M. L. (2004). *Environmental Monitoring and Characterization*. Elsevier Academic Press. http://www.123library.org/book_details/?id=35782

- ASC Scientific. (2023). *W.F. McCullough Geotechnical Gauge—Soils Classification Reference Chart—ASC Scientific*. <https://www.ascscientific.com/geology-field-equipment/reference-books-charts/geotechnical-gauge/>
- Australian Bureau of Meteorology. (2020a). *Climate statistics for Australian locations—St George Qld*. http://www.bom.gov.au/climate/averages/tables/cw_043034.shtml
- Australian Bureau of Meteorology. (2020b). *The Indian Ocean Dipole*. Bureau of Meteorology. <http://www.bom.gov.au/climate/enso/history/ln-2010-12/IOD-what.shtml>
- Australian Bureau of Meteorology. (2022, April 17). *Daily Rainfall—043109—Bureau of Meteorology*. http://www.bom.gov.au/jsp/ncc/cdio/weatherData/av?p_nccObsCode=136&p_display_type=dailyDataFile&p_startYear=&p_c=&p_stn_num=043109
- Australian Bureau of Meteorology. (2023). *Climate statistics for Australian locations—St George Airport*. http://www.bom.gov.au/climate/averages/tables/cw_043109_All.shtml
- Australian Bureau of Statistics. (2016). *2016 Census QuickStats: St George (Qld)*. https://quickstats.censusdata.abs.gov.au/census_services/getproduct/census/2016/quickstat/SSC32664
- Baloloy, A. B., Blanco, A. C., Candido, C. G., Argamosa, R. J. L., Dumalag, J. B. L. C., Dimapilis, L. L. C., & Paringit, E. C. (2018). Estimation of mangrove forest aboveground biomass using multispectral bands, vegetation indices and biophysical variables derived from optical satellite imageries: rapideye, planetscope and sentinel-2. *ISPRS Annals of Photogrammetry, Remote Sensing and Spatial Information Sciences*, IV-3, 29–36. <https://doi.org/10.5194/isprs-annals-IV-3-29-2018>

- Bian, J., Zhang, Z., Chen, J., Chen, H., Cui, C., Li, X., Chen, S., & Fu, Q. (2019). Simplified Evaluation of Cotton Water Stress Using High Resolution Unmanned Aerial Vehicle Thermal Imagery. *Remote Sensing*, *11*(3), 267. <https://doi.org/10.3390/rs11030267>
- Blue Marble Geographics. (2020). *Global Mapper* (22.0) [Computer software]. Blue Marble Geographics LLC. www.GlobalMapper.com
- Braun, A. (2021). *Sentinel-1 Toolbox—Synergetic use of radar and optical data*. Skywatch Space Applications Inc.
[http://step.esa.int/docs/tutorials/S1TBX%20Synergetic%20use%20of%20S1%20\(SAR\)%20and%20S2%20\(optical\)%20data%20Tutorial.pdf](http://step.esa.int/docs/tutorials/S1TBX%20Synergetic%20use%20of%20S1%20(SAR)%20and%20S2%20(optical)%20data%20Tutorial.pdf)
- Brinkhoff, J., Hornbuckle, J., & Barton, J. (2018). Assessment of Aquatic Weed in Irrigation Channels Using UAV and Satellite Imagery. *Water*, *10*(11), 1497.
<https://doi.org/10.3390/w10111497>
- Bureau of Meteorology. (2020b). *The Indian Ocean Dipole*. Bureau of Meteorology.
<http://www.bom.gov.au/climate/enso/history/ln-2010-12/IOD-what.shtml>
- Bureau of Meteorology. (2021). *Climate statistics for Australian locations*.
http://www.bom.gov.au/climate/averages/tables/cw_043109.shtml
- Bureau of Statistics. (2021). *2016 Census QuickStats: Emerald (Qld)*.
https://quickstats.censusdata.abs.gov.au/census_services/getproduct/census/2016/quickstat/SSC30982
- Butterworth, K. (2016, September 8). *Dryland Option for St George Growers*. Queensland Country Life. <http://www.queenslandcountrylife.com.au/story/4151062/dryland-option-for-st-g-growers/>
- Camra, G., Souza, R. C. M., Freitas, U. M., & Garrido, J. (1996). SPRING: Integrating Remote Sensing and GIS by object-oriented data modelling. *Computers and Graphics*, *20*(3), 395–403.

- Carlson, T. N., & Petropoulos, G. P. (2019). A new method for estimating of evapotranspiration and surface soil moisture from optical and thermal infrared measurements: The simplified triangle. *International Journal of Remote Sensing*, 40(20), 7716–7729. <https://doi.org/10.1080/01431161.2019.1601288>
- CASA. (2019, June 25). *Drone Safety Rules*. Civil Aviation Safety Authority; Civil Aviation Safety Authority. <https://www.casa.gov.au/drones/rules/drone-safety-rules>
- CFI Education Inc. (2022). *R-Squared*. Corporate Finance Institute. <https://corporatefinanceinstitute.com/resources/knowledge/other/r-squared/>
- Chatelard, C., Legoff, I., Serra, G., Munoz, J. S., Krapez, J.-C., Mazel, C., Olichon, V., Polo, J. B., Frederic, Y.-M., Helias, F., & Barillot, P. (2019). Leak Detection in Water Transmission Systems by Multispectral Remote Sensing With Airplane and UAV. *IGARSS 2019 - 2019 IEEE International Geoscience and Remote Sensing Symposium*, 7124–7127. <https://doi.org/10.1109/IGARSS.2019.8900288>
- Chen, A., Orlov-Levin, V., & Meron, M. (2018). Applying High-Resolution Visible-Channel Aerial Scan of Crop Canopy to Precision Irrigation Management. Proceedings of 2nd International Electronic Conference on Remote Sensing, 22 March–5 April 2018. <https://doi.org/10.3390/ecrs-2-05148>
- Chen, H. (2023, January 12). *Köppen climate classification*. Hans Chen. <http://hanschen.org/koppen>
- Civil Engineering. (2019). The Unified Soil Classification System (USCS). *Civil Engineering*. <https://www.civilengineeringx.com/geotechnical-engineering/the-unified-soil-classification-system-uscs/>
- Climate-Data.org. (2022). *St George climate: Average Temperature, weather by month, St George weather averages—Climate-Data.org*. <https://en.climate-data.org/oceania/australia/queensland/st-george-765372/>

Cook, B. G. (2007). *Factsheet—Buffel grass*.

https://keys.lucidcentral.org/keys/v3/pastures/Html/Bufel_grass.htm

Corporate Financial Institute. (2021). *P-value*. Corporate Finance Institute.

<https://corporatefinanceinstitute.com/resources/knowledge/other/p-value/>

Cruzan, M. B., Weinstein, B. G., Grasty, M. R., Kohn, B. F., Hendrickson, E. C., Arredondo,

T. M., & Thompson, P. G. (2016). Small Unmanned Aerial Vehicles (Micro-Uavs,

Drones) in Plant Ecology. *Applications in Plant Sciences*, 4(9), 1600041.

<https://doi.org/10.3732/apps.1600041>

Cubert-GmbH. (2020). ULTRIS X20—Hyperspectral UV-VIS-NIR Video Camera. *Cubert-*

GmbH. <https://cubert-gmbh.com/product/ultris-x20-hyperspectral/>

Department of Natural Resources, Mines and Energy. (2017). *St George Qld Irrigation*

channel line data [Map]. Queensland Government.

DJI. (2021). *P4 Multispectral—Specifications—DJI*. DJI Official. [https://www.dji.com/au/p4-](https://www.dji.com/au/p4-multispectral/specs)

[multispectral/specs](https://www.dji.com/au/p4-multispectral/specs)

DJI Industries Limited. (2021). *P4 Multispectral—DJI*. DJI Official.

<https://www.dji.com/au/p4-multispectral>

DJI Technology Co., Limited. (2022). *DJI GS Pro—DJI*. DJI Official.

<https://www.dji.com/au/ground-station-pro>

DroneCode Inc. (2020). *Introduction · MAVLink Developer Guide*. <https://mavlink.io/en/>

Dualem Inc. (2022). DUALEM Products. *DUALEM.COM*. <https://dualem.com/products/>

Dufek, J., Traore, S., Griffin, Maurice, Murphy, Robin, & Fipps, Guy. (2017, May 9).

Detection and Localization of Irrigation Canal Leaks Using Small Unmanned Aerial Systems at Low Altitude. *Association for Unmanned Vehicle Systems International*.

AUVSI XPONENTIAL, Texas A & M University.

- Earth Observing System. (2017, October 17). *NDVI: Normalized Difference Vegetation Index for Agriculture*. <https://eos.com/make-an-analysis/ndvi/>
- EMTOMO. (2023). *Products*. <http://www.emtomo.com/home/>
- Enterprise, D. J. I. (2022). *Why RTK Hardware is Here to Stay*. <https://enterprise-insights.dji.com/blog/rtk-real-time-kinematics>
- European Space Agency. (2015). *Sentinel 2 User Handbook* (1st ed.). European Space Agency. <https://sentinal.esa.int>
- European Space Agency. (2020). *Copernicus Satellite System*. <https://www.copernicus.eu/en>
- European Space Agency. (2021). *Sentinel-2—Missions—Sentinel Online—Sentinel*. <https://sentinel.esa.int/web/sentinel/missions/sentinel-2>
- European Space Agency. (2020). *SNAP Sentinel Toolbox application*. <http://step.esa.int/main/download/snap-download/>
- European Space Agency (1). (2021, April 1). *Sentinel-1—Mission Objectives—Sentinel Online—Sentinel*. <https://sentinel.esa.int/web/sentinel/missions/sentinel-1/mission-objectives>
- FarmOnLine Inc. (2021). *St George daily rain summaries*. <http://www.farmonlineweather.com.au/station.jsp?lt=site&lc=43109&list=rb>
- Geoscience Australia. (2019, May 7). *Topographic Maps* (Commonwealth of Australia). Australian Government\; Geoscience Australia. <https://www.ga.gov.au/scientific-topics/national-location-information/topographic-maps-data/topographic-maps>
- Gillies, R. R., Kustas, W. P., & Humes, K. S. (1997). A verification of the “triangle” method for obtaining surface soil water content and energy fluxes from remote measurements of the Normalized Difference Vegetation Index (NDVI) and surface e. *International Journal of Remote Sensing*, 18(15), 3145–3166. <https://doi.org/10.1080/014311697217026>

- Gitelson, A. A., Kaufman, Y. J., & Merzlyak, M. N. (1996). Use of a green channel in remote sensing of global vegetation from EOS-MODIS. *Remote Sensing of Environment*, 58(3), 289–298.
- Gitelson, A. A., Viña, A., Verma, S. B., Rundquist, D. C., Arkebauer, T. J., Keydan, G., Leavitt, B., Ciganda, V., Burba, G. G., & Suyker, A. E. (2006). Relationship between gross primary production and chlorophyll content in crops: Implications for the synoptic monitoring of vegetation productivity. *Journal of Geophysical Research*, 111(D8), D08S11. <https://doi.org/10.1029/2005JD006017>
- Gitelson, A. A., & Merzlyak, M. N. (1998). Remote sensing of chlorophyll concentration in higher plant leaves. *Advances in Space Research*, 22(5), 689–692.
[https://doi.org/10.1016/S0273-1177\(97\)01133-2](https://doi.org/10.1016/S0273-1177(97)01133-2)
- Goulburn_Murray Water Ltd. (2012). *TECHNICAL MANUAL FOR THE QUANTIFICATION OF WATER SAVINGS IN IRRIGATION WATER DISTRIBUTION SYSTEMS* (No. 4; p. 130). Victorian Government.
https://www.water.vic.gov.au/_data/.../Technical-Manual-Version-4.4-FINAL.pdf
- Gouri, L., and Manjula, K. R. (2019). Evaluation of Various Vegetation Indices for Multispectral Satellite Images. *International Journal of Innovative Technology and Exploring Engineering*, 8(10), 3494–3500.
<https://doi.org/10.35940/ijitee.J9195.0881019>
- Guo, Y., Senthilnath, J., Wu, W., Zhang, X., Zeng, Z., & Huang, H. (2019). Radiometric Calibration for Multispectral Camera of Different Imaging Conditions Mounted on a UAV Platform. *Sustainability*, 11(4), 978. <https://doi.org/10.3390/su11040978>
- Hall, T. (2019, April 18). DJI Drones Need This Many GPS Satellites to Fly. *Let Us Drone*.
<https://www.letusdrone.com/dji-drones-need-this-many-gps-satellites-to-fly/>

Harris Corporation. (2015). *ENVI (5.3.1)* [Windows]. Exelis Visual Information Systems Inc.

<https://www.l3harrisgeospatial.com>

Harris Geospatial Solutions Inc. (2021). *High Resolution Satellite Imagery | High-Res*

Satellite Images | L3Harris Geospatial. High Resolution Satellite Imagery.

<https://www.l3harrisgeospatial.com/Data-Imagery/Satellite-Imagery/High-Resolution>

Harris Geospatial Systems. (2018). *Broadband Greenness*.

<https://www.harrisgeospatial.com/docs/BroadbandGreenness.pdf>

Henrich, V., & Bruser, K. (2022). *IDB - Index DataBase*. <https://www.indexdatabase.de/>

Huang, J., Scudiero, E., Choo, H., Corwin, D. L., & Triantafilis, J. (2016). Mapping soil moisture across an irrigated field using electromagnetic conductivity imaging.

Agricultural Water Management, 163, 285–294.

<https://doi.org/10.1016/j.agwat.2015.09.003>

Huang, Y., Fipps, G., Maas, S. J., & Fletcher, R. S. (2010). Airborne remote sensing for detection of irrigation canal leakage. *Irrigation and Drainage*, 59(5), 524–534.

<https://doi.org/10.1002/ird.511>

Ibrahim, J.T, Waskitho, N. T., & Ma'mun, S. R. (2017). Survey of irrigation area using micro unmanned aerial vehicle (micro-uav) in Gumbasa irrigation area. *Agricultural Social*

Economic Journal, 17(1), 1–5. <https://doi.org/10.21776/ub.agrise.2017.017.1.1>

Institute of Public Work Engineering Australasia. (2020). *Public works and drones – the sky's the limit*. <https://www.ipwea.org/blogs/intouch/2018/10/03/public-works-and-drones-the-skys-the-limit>,

<https://www.ipwea.org/blogs/intouch/2018/10/03/public-works-and-drones-the-skys-the-limit>

<https://www.ipwea.org/blogs/intouch/2018/10/03/public-works-and-drones-the-skys-the-limit>

Huang, Y., Fipps, G., Maas, S. J., & Fletcher, R. S. (2010). Airborne remote sensing for detection of irrigation canal leakage. *Irrigation and Drainage*, 59(5), 524–534.

<https://doi.org/10.1002/ird.511>

- Kandylakis, Z., Falagas, A., Karakizi, C., & Karantzalos, K. (2020). Water Stress Estimation in Vineyards from Aerial SWIR and Multispectral UAV Data. *Remote Sensing*, 12(15), 2499. <https://doi.org/10.3390/rs12152499>
- King, P. (2021, May 12). *Goulburn- Murray Water's channel lengths* [Personal communication].
- L3Harris Geospatial Solutions, Inc. (2022). *Introduction to ENVI LiDAR*.
<https://www.l3harrisgeospatial.com/docs/introductionlidar.html>
- Landa, E. R. (2004). Albert H Munsell: A SENSE OF COLOR AT THE INTERFACE OF ART AND SCIENCE. *Soil Science*, 169(2), 83–89.
<https://doi.org/10.1097/01.ss.0000117789.98510.30>
- Mallawa Irrigation Limited. (2018). *About Mallawa Irrigation Limited*. Mallawa Irrigation.
<https://mallawairrigation.com.au/about>
- Mallawa Irrigation Ltd. (2022). *Mallawa Irrigation Limited 2023 Pricing*. Mallawa Irrigation. <https://mallawairrigation.com.au/2023-pricing>
- McCulloch, W. F. (2020). *Geotechnical Gauge*. Amazon Inc.
- McLeod, S. A. (2019). *P-Value and Statistical Significance | Simply Psychology*.
<https://www.simplypsychology.org/p-value.html>
- MicaSense Limited. (2018). *Detecting Disease Earlier: The Importance of the Red Edge Band*. <https://micasense.com/detecting-disease-earlier-the-importance-of-the-red-edge-band/>
- Minnesota Department of Natural Resources. (2021). *DNRGPS (6.1.0.6) Computer software*.
- NSW Department of Sustainable Natural Resources. (1990). *SOIL SURVEY STANDARD TEST METHOD SOIL MOISTURE CONTENT*.
<https://www.environment.nsw.gov.au/resources/soils/testmethods/mc.pdf>

NSW Dept of Primary Industry. (2022). *NSW WeedWise*.

<https://weeds.dpi.nsw.gov.au/Weeds/Details/274>

Park, S., Ryu, D., Fuentes, S., Chung, H., O'Connell, M., & Kim, J. (2021). Mapping Very-High-Resolution Evapotranspiration from Unmanned Aerial Vehicle (UAV) Imagery. *ISPRS International Journal of Geo-Information*, 10(4), 211.

<https://doi.org/10.3390/ijgi10040211>

Plyer, A. (2023). *Gefolki Software* [Jupyter Notebook]. <https://github.com/aplyer/gefolki>
(Original work published 2016)

Position Partners. (2021). Agisoft Metashape Formerly Photoscan Available At Position Partners. *Position Partners*. <https://www.positionpartners.com.au/product/agisoft-metashape/>

Price, J. C. (1980). The Potential of Remotely Sensed Thermal Infrared Data to Infer Surface Soil Moisture and Evaporation. *WATER RESOURCES RESEARCH*, 16(4), 787–795.

Qi, J., Chehbouni, A., Huete, A. R., Kerr, Y. H., & Sorooshian, S. (1994). A modified soil adjusted vegetation index. *Remote Sensing of Environment*, 48(2), 119–126.

[https://doi.org/10.1016/0034-4257\(94\)90134-1](https://doi.org/10.1016/0034-4257(94)90134-1)

Qld Department of Agriculture, Forests and Fisheries. (2013). *Rhodes grass*.

<https://www.daf.qld.gov.au/business-priorities/agriculture/plants/crops-pastures/pastures/rhodes-grass>

Queensland Irrigation and Water Supply Commission. (2014a). *St George Irrigation Project-Proposed Extensions-Soil Associations* [Map]. Queensland Government.

Ruwaimana, M., Satyanarayana, B., Otero, V., M. Muslim, A., Syafiq A., M., Ibrahim, S., Raymaekers, D., Koedam, N., & Dahdouh-Guebas, F. (2018). The advantages of using drones over space-borne imagery in the mapping of mangrove forests. *PLOS ONE*, 13(7), e0200288. <https://doi.org/10.1371/journal.pone.0200288>

SAS Planet Development Team. (2021). *SAS Planet* (200606.10075) [Windows].

<http://sasqis.org>

Sonobe, R., & Wang, Q. (2017). Towards a Universal Hyperspectral Index to Assess Chlorophyll Content in Deciduous Forests. *Remote Sensing*, 9(3), 191.

<https://doi.org/10.3390/rs9030191>

Sozzi, M., Martinello, F., Pessuolo, A., & Sartori, L. (2018). *Benchmark of Satellites Image Services for Precision Agricultural use*.

Sphere Drones Australia. (2022). *MicaSense Multispectral Sensors—RedEdge-P, Altum-PT, RedEdge-MX*. Sphere Drones. <https://spheredrones.com.au/pages/micasense-multispectral-sensors>

Spires, J. (2021, March 31). DJI: Best drones, history, technology, and more. *DroneDJ*.

<https://dronedj.com/guides/dji/>

Standards Australia. (2022). *AS 1289.B1.1-1977 | Standards Australia Methods of testing soil for engineering purposes, Part B1.1: Soil moisture content tests—Determination of the moisture content of a soil—Oven drying method (standard method)*.

<https://store.standards.org.au/product/as-1289-b1-1-1977>

SunWater, Queensland. (2021). *St George Water Supply Scheme*.

<http://www.sunwater.com.au/schemes/st-george>

SunWater, Queensland. (2021c). *Sunwater: Storage Levels*.

https://storagelevels.sunwater.com.au/win/reports/win_storages.htm

SunWater Queensland. (2022). *Sunwater: Storage Levels*.

https://storagelevels.sunwater.com.au/win/reports/win_storages.htm

Sykas, D. (2022). *Vegetation Indices A review of commonly used spectral indices*. GIS and Earth Observation University. Retrieved June 25, 2021, from

<https://www.geo.university/pages/vegetation-indices-a-review-of-commonly-used-spectral-indices>

- Sylvester, G., Food and Agriculture Organization of the United Nations, & International Telecommunication Union. (2018). *E-agriculture in action: Drones for agriculture*.
- Tagari, H., & Ben-Ghedalia, D. (1977). The digestibility of Rhodes grass (*Chloris gayana*) in relation to season and proportion of the diet of sheep. *The Journal of Agricultural Science*, 88(1), 181–185. <https://doi.org/10.1017/S002185960003392X>
- Tiner, R. W., Lang, M. W., & Klemas, V. (Eds.). (2015). *Remote sensing of wetlands: Applications and advances*. CRC Press, Taylor & Francis Group.
- Tong, A., & He, Y. (2017). Estimating and mapping chlorophyll content for a heterogeneous grassland: Comparing prediction power of a suite of vegetation indices across scales between years. *ISPRS Journal of Photogrammetry and Remote Sensing*, 126, 146–167. <https://doi.org/10.1016/j.isprsjprs.2017.02.010>
- United States Geological Survey. (2021). *Landsat 8*. https://www.usgs.gov/core-science-systems/nli/landsat/landsat-8?qt-science_support_page_related_con=0#qt-science_support_page_related_con
- US Department of Transportation. (2017, June 27). *AASHO Road Test—Interstate System—Highway History—Federal Highway Administration*. <https://www.fhwa.dot.gov/infrastructure/50aasho.cfm>
- US Government. (2021). *US Patent Full-Text Database Boolean Search*. <http://patft.uspto.gov/netahtml/PTO/search-bool.html>
- Wang, S., Garcia, M., Ibrom, A., Jakobsen, J., Josef Köppl, C., Mallick, K., Looms, M., & Bauer-Gottwein, P. (2018). Mapping Root-Zone Soil Moisture Using a Temperature–Vegetation Triangle Approach with an Unmanned Aerial System: Incorporating Surface

Roughness from Structure from Motion. *Remote Sensing*, 10(12), 1978.

<https://doi.org/10.3390/rs10121978>

Wilson, S. D., Seed, H. B., & Peck, R. B. (1982). Arthur Casagrande, 1902–1981 a tribute.

Géotechnique, 32(2), 87–94. <https://doi.org/10.1680/geot.1982.32.2.87>

Wingtra AG. (2019, December 19). *What are the best mapping drones in wind?* Wingtra.

<https://wingtra.com/best-mapping-drones-in-wind/>

Witczuk, J., Pagacz, S., Zmarz, A., & Cypel, M. (2018). Exploring the feasibility of

unmanned aerial vehicles and thermal imaging for ungulate surveys in forests—

Preliminary results. *International Journal of Remote Sensing*, 39(15–16), 5504–5521.

<https://doi.org/10.1080/01431161.2017.1390621>

Yang, Y., Gao, W., Guo, S., Mao, Y., & Yang, Y. (2019). Introduction to BeiDou-3

navigation satellite system. *Navigation*, 66(1), 7–18. <https://doi.org/10.1002/navi.291>

Zare, E., Li, N., Khongnawang, T., Farzamian, M., & Triantafilis, J. (2020). Identifying

Potential Leakage Zones in an Irrigation Supply Channel by Mapping Soil Properties

Using Electromagnetic Induction, Inversion Modelling and a Support Vector Machine.

Soil Systems, 4(2), 25. <https://doi.org/10.3390/soilsystems4020025>